REPORT DOCUMENTATION PAGE		READ INSTRUCTIONS BEFORE COMPLETING FORM
1. REPORT NUMBER RPI Math. Rep. No. 152	2. GOVT ACCESSION NO.	3. RECIPIENT'S CATALOG NUMBER
4. TITLE (and Subtitle) Ray transmissions over a sloping bottom in shallow water		5. TYPE OF REPORT & PERIOD COVERED
		6. PERFORMING ORG. REPORT NUMBER
7. AUTHOR(s) M. J. Jacobson, W. L. Siegmann, and T. H. Rousseau		8. CONTRACT OR GRANT NUMBER(s) N00014-76-C-0288
9. PERFORMING ORGANIZATION NAME AND ADDRESS Rensselaer Polytechnic Institute Troy, New York 12180-3590		10. PROGRAM ELEMENT, PROJECT, TASK AREA & WORK UNIT NUMBERS NR 386-606
11. CONTROLLING OFFICE NAME AND ADDRESS Office of Naval Research, Code 425 Department of the Navy Arlington, Virginia 22217		12. REPORT DATE 1 August 1985
		13. NUMBER OF PAGES 49
14. MONITORING AGENCY NAME & ADDRESS(if different from Controlling Office)		15. SECURITY CLASS. (of this report)
		15a. DECLASSIFICATION·DOWNGRADING SCHEDULE

16. DISTRIBUTION STATEMENT (of this Report)

This document has been approved for public release and sale; its
distribution is unlimited

17. DISTRIBUTION STATEMENT (of the abstract entered in Block 20, if different from Report)

18. SUPPLEMENTARY NOTES

19. KEY WORDS (Continue on reverse side if necessary and identify by block number)

20. ABSTRACT (Continue on reverse side if necessary and identify by block number)

The effects of a sloping bottom on acoustic transmissions, between a
source and receiver at arbitrary but fixed locations, are investigated using
ray theory. An isospeed channel is assumed, and bottom angles up to about 3°
are considered. Sloping bottom influence on per-ray quantities, including
travel time and transmission loss, are examined for cw transmissions. Signi-
ficant variations are shown to occur, such as travel time changes of more
than 200 ms over ranges of about six km. Per-ray transmission loss is found

DD FORM 1473 EDITION OF 1 NOV 65 IS OBSOLETE
1 JAN 73
S/N 0102-LF-014-6601

to be influenced strongly by bottom slope, the amount of influence depending upon source-receiver bearing and the bottom loss model used. Variations of more than 20 dB are demonstrated. Effects of a sloping bottom on the total acoustic field are examined also, and the results compared with those for a horizontal bottom. Finally, a simple model of a shallow water front is super-posed over the sloping bottom, and travel time is investigated. The sloping bottom effectcan induce travel time changes more than 300% larger than the frontal effect for different source-receiver geometries and bottom inclinations.

Ray Transmissions over a Sloping
Bottom in Shallow Water

by

M. J. Jacobson, W. L. Siegmann
and T. H. Rousseau

Department of Mathematical Sciences

Rensselaer Polytechnic Institute

Troy, New York 12181

RPI Math. Rep. No. 152

August 1, 1985

ABSTRACT

The effects of a sloping bottom on acoustic transmissions, between a source and receiver at arbitrary but fixed locations, are investigated using ray theory. An isospeed channel is assumed, and bottom angles up to about 3° are considered. Sloping bottom influence on per-ray quantities, including travel time and transmission loss, are examined for cw transmissions. Significant variations are shown to occur, such as travel time changes of more than 200 ms over ranges of about six km. Per-ray transmission loss is found to be influenced strongly by bottom slope, the amount of influence depending upon source-receiver bearing and the bottom loss model used. Variations of more than 20 dB are demonstrated. Effects of a sloping bottom on the total acoustic field are examined also, and the results compared with those for a horizontal bottom. Finally, a simple model of a shallow water front is superposed over the sloping bottom, and travel time is investigated. The sloping bottom effect can induce travel time changes more than 300% larger than the frontal effect for different source-receiver geometries and bottom inclinations.

1

INTRODUCTION

Shallow water in the world's oceans occurs along continental margins and in many of the seas.[1] Continental margins are subdivided into the continental shelf, a region of gently sloping bottoms with slopes of 0° to 3°, and the continental slope or shelf break region, where water depth increases rapidly and bottom inclination can be as much as 5°.[1,2] Acoustic transmission in shallow water is significantly different from deep water transmission with the former being characterized by stronger bottom interaction and somewhat shorter ranges (see, for example, Ref. 3). Acoustic models of the shallow ocean vary in complexity from a simple constant depth, isospeed medium to one in which depth, sound speed, and bottom properties vary spatially.[4]

A variety of papers have shown certain consequences of shallow ocean environmental features on acoustic transmissions. For example, both ray and mode theories were used[5,6] to indicate influences of sloping bottoms on signal intensity and on horizontal trajectories of propagating modes. A method[7] for studying the horizontal propagation of local normal modes has been applied to a wedge shaped duct, which affects individual mode trajectories and eigenvalues differently. Accurate analytic approximations from ray theory, for ray geometry, travel time, and spreading loss, have been obtained,[8,9] but only for the strictly two-dimensional propagation directly up-or downslope. Transmission losses and shadow zones for an isospeed wedge shaped duct have been described for medium range propagation using geometric acoustics and normal modes.[10] The three-dimensional nature of acoustic propagation induced by variable bottom topography has been shown to strongly influence horizontal ray trajectories and shadow zone locations.[11,12] Recent studies have concentrated on application of the parabolic approximation to shallow water sloping bottom oceans,[13,14] to show modal cutoff for upslope

propagation.[15] Also, modal coupling has been considered,[16] and different methods for wave propagation over an inclined bottom have been developed[17] and adapted.[18,19] Relationships among propagation theories have been clarified in detail (as in Ref. 20). In addition, some deep water studies have used ray theory to demonstrate inclined bottom effects between fixed sources and receivers.[21,22]

The purpose of this paper is to study sound transmission in shallow water over a sloping bottom when source and receiver are located at arbitrary positions in the sound channel, but at relatively short range. We consider cw signals of sufficiently high frequency to permit the use of ray theory. The influence of the sloping bottom on acoustic quantities is developed in a constant sound speed medium with a Mackenzie bottom model.[23] Other bottom models may be used in shallow water (see, for instance, Ref. 24) with similar results. A sound channel with horizontal surface and bottom dictates two-dimensional ray paths in the vertical plane containing the source and receiver. Imposition of a plane, sloping bottom necessitates consideration of three-dimensional ray paths for other than directly up- or downslope, as is well known.

The principal novelty of this paper is the development of analytic approximations for three-dimensional ray geometry, travel time, and per-ray and total-field loss between a fixed source and receiver. Our study of ray geometric properties and of certain acoustical effects of three-dimensional ray paths produces new results. For instance, our formulas facilitate interpretation of acoustic variations which result from changes in source-receiver location and bottom inclination. Another feature of this paper is an appraisal of the relative acoustic significance of a sloping bottom and a shallow ocean front, using results of another study.[25] In numerical examples we use frontal parameters which are similar to those of the Slope Front in the North Atlantic Ocean. Enough

parameter variations are considered so that our results are applicable to a variety of ocean environments. Finally, we remark that detailed comparisons of our results with those in the previous studies cited above are not attempted in this paper. This is because different acoustical quantities are typically emphasized, and because our results are applicable to shorter range transmissions, while previous studies are primarily applicable to longer ranges. However, it should be noted that there is strong qualitative agreement between level curves of transmission loss in this paper and those calculated by Bradley[10], which were obtained using normal mode theory and which apply at longer ranges.

In Sec. I we describe ray geometry determined by regular perturbations from an isospeed sound channel with horizontal surface and bottom. It is shown how ray geometry depends upon bottom inclination, source-receiver bearing relative to the maximum gradient of bottom slope and range. Results are used in Sec. II to express travel time and spreading loss in terms of bottom angle and bearings. Then, a Mackenzie bottom model is used in an examination of per-ray transmission loss. Incoherent total-field transmission loss is considered also, and the sloping bottom influence is discussed. Section III studies the effect of a sloping bottom superimposed on propagation through a simple frontal model. Ray geometry and travel time expressions are derived, and the relative significance of the sloping bottom and front are illustrated. Finally, we summarize our results in Sec. IV.

I. MODEL DESCRIPTION AND RAY GEOMETRY

The bottoms on the continental shelf and in shelf break regions are commonly and most easily modelled as planes with angles of inclination of up to about $5°$.[4,8,9] In this paper, we model the ocean above the continental shelf as a channel bounded above by a horizontal surface and below by a plane having an angle of inclination α. Subsequently, we will use radian measure for this and other angular quantities. In order to concentrate on the sloping bottom effect, we initially suppress oceanic variations, taking the water to be stationary and to have constant sound speed c. The influence of the sloping bottom will be investigated using ray theory and a Mackenzie bottom interaction model.[23]

Suppose that an omnidirectional sound source S and a point receiver R are located at arbitrary depths h_S and h_R in an ocean channel of depth d_R at R. We establish a right-handed Cartesian coordinate system with origin on the surface over R, with depth z increasing downward, and with x increasing directly upslope (shoreward), as shown in Fig. 1(a). The bottom angle α is nonnegative and measured from the horizontal, and the relative bearing β of S from R is measured positively clockwise from the y-axis as shown in Fig. 1(b). It is the angle $\beta(-\pi < \beta \leq \pi)$, then, which specifies propagation in a convergent or divergent channel. The range R is the horizontal distance separating S and R. We use N to designate the total number of bottom reflections between S and R for a given ray, and we number bottom reflections sequentially from S to R by $1,2,...,N$. A ray lobe is that portion of a ray path between successive bottom reflections, and the lobe is numbered with the smaller of its bottom reflection numbers (i.e., lobe k is that portion of the ray path between bottom reflections k and k + 1). Lobe zero is the (typically partial)

lobe between S and the first bottom reflection, while lobe N is the (typically partial) lobe between the last (Nth) bottom reflection and R. We designate the water depth at S by d_S and the depth at bottom reflection $k(1 \leq k \leq N)$ by h_{kN}.

The altitudinal angles of a ray at S and R are Θ_{SN} and Θ_{RN}, respectively, measured positively downward from the horizontal. In lobe k $(1 \leq k \leq N-1)$, Θ_{kN} is the positive altitudinal angle of the ray after its surface reflection; Θ_{oN} is the altitudinal ray angle in lobe zero as the ray path approaches the first bottom reflection; Θ_{NN} is that angle in lobe N after surface reflection, if such a reflection occurs. For arbitrary source and receiver depths and fixed N, there will, in general, be four rays connecting S to R. We introduce the parameter $\sigma_S(\sigma_R)$ which is +1 if Θ_{SN} (Θ_{RN}) > 0 and is -1 if Θ_{SN} (Θ_{RN}) < 0. We relate altitudinal angles by

$$\Theta_{SN} = \sigma_S \Theta_{oN} \qquad (1a)$$

and

$$\Theta_{RN} = \sigma_R \Theta_{NN} \qquad (1b)$$

In Fig. 1, we show schematically a ray with N = 3, for which $\sigma_S = -1$ and $\sigma_R = +1$. Each ray lobe lies in a single vertical plane and specular reflection insures that, in general, adjacent lobes lie in different vertical planes, giving rise to three-dimensional ray paths. The azimuthal angle in lobe k(0 $\leq$ k $\leq$ N) of a ray is ϕ_{kN}, measured in the same way as β. The projection of the ray path in lobe k onto a horizontal plane is called L_{kN}. In general, N-dependent quantities, such as θ_{SN} and h_{kN}, are functions of σ_S and σ_R. For simplicity, however, we will suppress this dependence in subsequent notation. Further, nondimensional quantities will be designated by a caret ($\wedge$), while

quantities associated with a sound channel having a horizontal bottom of depth d_R will be indicated by an overbar.

For fixed source and receiver locations, fixed N, and specified σ_S and σ_R, we facilitate the determination of the geometry of a ray by specifying the unit vector tangent to the ray at S, $\underline{\Lambda}_{SN}$, and at R, $\underline{\Lambda}_{RN}$. In lobe $k(0 \leq k \leq N)$, the unit vector tangent to the ray approaching the bottom reflection is $\underline{\Lambda}'_{kN}$. Although $\underline{\Lambda}'_{NN}$ is not actually present on the physical ray when $\sigma_R = -1$, it is a computational convenience; a similar statement applies to $\underline{\Lambda}_{oN}$ when $\sigma_S = +1$. Unit ray tangents may be written as

$$\underline{\Lambda}_{SN} = \begin{pmatrix} \cos \Theta_{SN} \sin \phi_{oN} \\ -\cos \Theta_{SN} \cos \phi_{oN} \\ \sin \Theta_{SN} \end{pmatrix}, \tag{2a}$$

$$\underline{\Lambda}_{RN} = \begin{pmatrix} \cos \Theta_{RN} \sin \phi_{NN} \\ -\cos \Theta_{RN} \cos \phi_{NN} \\ \sin \Theta_{RN} \end{pmatrix}, \tag{2b}$$

and

$$\underline{\Lambda}_{kN} = \begin{pmatrix} \cos \Theta_{kN} \sin \phi_{kN} \\ -\cos \Theta_{kN} \cos \phi_{kN} \\ -\sin \Theta_{kN} \end{pmatrix}, \quad 0 \leq k \leq N. \tag{2c}$$

The effect of a boundary reflection on the unit tangent vector to a ray is normally written as a vector equation, with the reflected tangent vector expressed as a linear combination of the incident unit tangent vector and a vector normal to the boundary.[26] This linear combination of vectors is a linear transformation of the incident ray tangent, and can be represented by a matrix.[27] The matrix of transformation $\underline{T}_T$ at a surface reflection, and that at a bottom reflection, $\underline{T}_B$, can be written as

$$\underline{T}_T = \begin{pmatrix} 1 & 0 & 0 \\ 0 & 1 & 0 \\ 0 & 0 & -1 \end{pmatrix} \tag{3a}$$

and

$$\underset{\sim}{T}_B = \begin{pmatrix} \cos 2\alpha & 0 & -\sin 2\alpha \\ 0 & 1 & 0 \\ -\sin 2\alpha & 0 & -\cos 2\alpha \end{pmatrix} . \tag{3b}$$

Ray tangents can now be related by

$$\underset{\sim}{\Lambda}'_{kN} = \underset{\sim}{T}_T \underset{\sim}{\Lambda}_{kN} \quad , \quad 0 \leq k \leq N , \tag{3c}$$

and

$$\underset{\sim}{\Lambda}'_{(k+1)N} = \underset{\sim}{T}_T \underset{\sim}{T}_B \underset{\sim}{\Lambda}'_{kN} \quad , \quad 0 \leq k \leq N-1 . \tag{3d}$$

Thus, we can relate $\underset{\sim}{\Lambda}'_{kN}$ to a ray tangent near R by

$$\underset{\sim}{\Lambda}'_{kN} = \left(\underset{\sim}{T}_B \underset{\sim}{T}_T \right)^{N-k} \underset{\sim}{\Lambda}'_{NN} \quad , \quad 0 \leq k \leq N-1 . \tag{4}$$

The ray tangent at S (or R), $\underset{\sim}{\Lambda}_{SN}$ (or $\underset{\sim}{\Lambda}_{RN}$), is $\underset{\sim}{\Lambda}_{0N}$ (or $\underset{\sim}{\Lambda}_{NN}$) if σ_S (or σ_R) = -1.

It is necessary to determine ray geometry in order to calculate travel time, spreading loss, and bottom loss. We first seek to determine the altitudinal and azimuthal angles of a ray tangent at S and R, and these quantities are then specified at any point on the ray path through Eq. (4). We write the x and y components of range in the form

$$R \sin \beta = \sum_0^N L_{kN} \sin \phi_{kN} \tag{5a}$$

and

$$R \cos \beta = \sum_0^N L_{kN} \cos \phi_{kN} . \tag{5b}$$

Now, the L_{kN} are related to water depth, ray angles, and bottom inclination by the equations

$$L_{ON} = (d_S - \sigma_S h_S)(\tan\Theta_{ON} + \tan\alpha \sin\phi_{ON})^{-1} , \tag{6a}$$

$$L_{kN} = 2h_{kN}(\tan\Theta_{kN} + \tan\alpha \sin\phi_{kN})^{-1} , \quad 1 \le k \le N-1 , \tag{6b}$$

and

$$L_{NN} = (d_R + \sigma_R h_R)(\tan\Theta_{NN} - \tan\alpha \sin\phi_{NN})^{-1} . \tag{6c}$$

Further, water depths at successive bottom reflections can be determined recursively from

$$h_{(k+1)N} = h_{kN}(\tan\Theta_{kN} - \tan\alpha \sin\phi_{kN})$$
$$\times (\tan\Theta_{kN} + \tan\alpha \sin\phi_{kN})^{-1} , \quad 1 \le k \le N-1 , \tag{6d}$$

with h_{1N} being given by

$$h_{1N} = (d_S \tan\Theta_{ON} + \sigma_S h_S \tan\alpha \sin\phi_{ON})$$
$$\times (\tan\Theta_{ON} + \tan\alpha \sin\phi_{ON})^{-1} . \tag{6e}$$

When Eqs. (6) are substituted into Eqs. (5) and (4) we have a system of non-linear coupled equations in the four angles Θ_{ON}, Θ_{NN}, ϕ_{ON}, and ϕ_{NN}. Equations (1) then give Θ_{SN} and Θ_{RN}. Since the system cannot be solved analytically, we proceed to perturb off known results[3] for an isospeed channel with constant depth d_R (i.e., $\alpha=0$). For $\alpha \ll 1$, we write

$$\Theta_{kN} = \overline{\Theta}_N + \Delta\Theta_{kN} , \quad 0 \le k \le N , \tag{7a}$$

and

$$\phi_{kN} = \beta + \Delta\phi_{kN} , \quad 0 \le k \le N , \tag{7b}$$

where $\overline{\Theta}_N$ is known from Ref. 3 to be

$$\tan \overline{\Theta}_N = \left[2N - \sigma_S \hat{h}_S + \sigma_R \hat{h}_R + 2H(\hat{n}_S-1)N \tan \alpha \right] \hat{R}^{-1} . \qquad (8)$$

In Eq. (8), depth and range parameters with carets are nondimensionalized with respect to d_R, $\hat{h}_S = h_S d^{-1}$, $\hat{h}_R = h_R d^{-1}$, and $\hat{R} = Rd^{-1}$, and H is the Heaviside function. The Heaviside function permits inclusion of the last term in Eq. (8) whenever source depth exceeds d_R.

When we substitute Eqs. (7) into Eqs. (2) and (4) and linearize in $\Delta\Theta_{kN}$, $\Delta\phi_{kN}$ and α, we obtain approximations for $\Delta\Theta_{kN}$ and $\Delta\phi_{kN}$ in terms of $\Delta\Theta_{oN}$ and $\Delta\phi_{oN}$. The approximations for $\Delta\Theta_{kN}$ and $\Delta\phi_{kN}$ are substituted first in Eqs. (6), and then in Eqs. (5), with linearization in small quantities at each step. Eventually we are able to approximate angular changes in the four ray angles at S and R, in the form

$$\Delta\Theta_{oN} \doteq -2N\alpha(N+\sigma_R\hat{h}_R)\hat{R}^{-1} \sin \beta \cos \overline{\Theta}_N \sin \overline{\Theta}_N , \qquad (9a)$$

$$\Delta\Theta_{NI} \doteq -2N\alpha\left[(N+\sigma_R\hat{h}_R)\hat{R}^{-1} \sin \beta \cos \overline{\Theta}_N \sin \overline{\Theta}_N - 2N \sin \beta \right] , \qquad (9b)$$

$$\Delta\phi_{oN} \doteq 2N\alpha(N+\sigma_R\hat{h}_R)\hat{R}^{-1} \cos \beta , \qquad (9c)$$

and

$$\Delta\phi_{NN} \doteq 2N\alpha\left[(N+\sigma_R\hat{h}_R)\hat{R}^{-1}-\tan \overline{\Theta}_N \right]\cos \beta . \qquad (9d)$$

Equations (9) are accurate provided $\overline{\Theta}_N$ is not too close to 0 or $\pi/2$ rad, so that unperturbed rays interacting with the bottom must not be too shallow or too steep. In order to assess the accuracy, approximations from Eqs. (9) were compared with numerical solution of the system of equations.[28] For example, with surfaced S and R, R = 5 km, α = 0.5°, β = -45°, d_R = 300 m, and rays with N = 1,2,...,5, approximations to altitudinal angles showed relative errors of less than 4%, while bearing approximations were accurate to within 6%.

The altitudinal angles of perturbed rays transmitted to a receiver upslope ($0 < \beta < \pi$) are shallower than their unperturbed ray counterparts, i.e. $\Delta\Theta_{oN} < 0$; yet the altitudinal arrival angles at R are steeper because of bottom interaction. Similarly, rays launched downslope ($-\pi < \beta < 0$) start more steeply than unperturbed rays, $\Delta\Theta_{oN} > 0$, and arrive at shallower angles. When S is directly across-slope from R ($\beta = 0, \pi$), altitudinal angles are insignificantly affected by bottom inclination as shown in Eqs. (9a) and (9b). The azimuthal changes indicated in Eqs. (9c) and (9d) show that the tendency of the sloping bottom to reflect a ray slightly downslope with each reflection is countered with a launch azimuth more upslope than the source bearing β. Thus, we see that $\Delta\phi_{oN}$ is positive for S in the first and second quadrants ($y > 0$), and negative for S in the third and fourth quadrants, of the xy-plane shown in Fig. 1. Of course, there is no azimuthal variation when the source is directly upslope ($\beta = \pi/2$) or directly downslope ($\beta = \pi/2$).

II. TRAVEL TIME AND TRANSMISSION LOSS

First, we develop and examine an expression for the travel time T_N for a ray with N bottom reflections (and with a specification of σ_S and σ_R). If S_N is the arc length of the ray, then

$$T_N = S_N/c = c^{-1} \sum_0^N L_{kN} \sec \Theta_{kN} . \tag{10a}$$

If we define ΔT_N to be the change in travel time from that in an ocean with horizontal bottom of depth d_R, $\overline{T}_N$, then

$$\Delta T_N = T_N - \overline{T}_N , \tag{10b}$$

where

$$\overline{T}_N = (R \sec \overline{\Theta}_N)c^{-1} . \tag{10c}$$

Using the angle changes of Eqs. (9) to approximate the L_{kN} in Eqs. (5), and substituting into Eqs. (10a) and (10b), it can be shown that, to first degree terms in α,

$$\Delta T_N \doteq 2N\alpha\overline{T}_N\{\sin \beta[N+\sigma_R\hat{h}_R]\hat{R}[\hat{R}^2+(2N + \sigma_S\hat{h}_S + \sigma_R\hat{h}_R)^2]^{-1}\} . \qquad (10d)$$

A suggestion of the accuracy of our approximation can be given for the parameter values used in Sec. I. In this case, the approximate travel time calculated from Eqs. (10b) and (10d) has been shown to vary with N from 3.1% to 11.1% of that predicted by Eq. (10a), in which results of the aforementioned numerical solution for ray geometry are used.

To illustrate travel time variations here, and variations in other acoustical quantities subsequently, we shall use the parameter values $d_R = 300$ m, $c = 1500$ ms^{-1}, and $\alpha = 2°$. For convenience, we shall take S and R in our numerical examples to be located on the surface. Other source and receiver depths have been shown to give rise to similar behavior in acoustical quantities. We note that S and R on the surface correspond to the values $\sigma_S = +1$ and $\sigma_R = -1$.

Figure 2 displays level curves of T_5 from Eqs. (10b)-(10d) for R fixed at the origin and for S at (x,y). The level curves are clearly skewed in the upslope direction. The observed x-axis symmetry can be seen to come from the $\sin \beta$ term in Eq. (10d). Also, the near-circularity of the level curves is explained by considering T_5 from Eq. (10b) as the polar equation of a Limaçon of Pascal, $r = b + a \sin \beta$, with $a \ll b$ after substituting Eqs. (10c) and (10d). Travel times for sources equidistant from R are generally longer when propagating upslope ($\beta > 0$) than when propagating downslope, with longest travel time corresponding to directly upslope transmission ($\beta = \pi/2$). When S is located in water of the same depth as that at R ($\beta = 0$ or π), travel times from sources equidistant from R are, of course, equal.

In Fig. 3, we allow S to assume successive positions along each of four paths, $P_1, \ldots, P_4$, which are shown in Fig. 2 and which have the same closest point of approach (CPA) to the source, 5 km. Path P_1 represents a track parallel to the shore upslope from R (sound propagates downslope). Path P_2 is similar, except that the track is downslope from R and the signal propagates upslope. Path P_3 represents a track directly upslope. A track at 45° across the slope is represented by path P_4. The symmetry of travel time T_5 about the x-axis can be seen on paths P_1 and P_2 in Fig. 3. In contrast, the asymmetry of T_5 about the y-axis on path P_3 is seen from the shift of the minimum away from CPA. This is caused by the fact that arc length is a minimum for a source location slightly upslope from $\beta = 0$. When compared to a constant depth ocean, $\alpha = 0$, it can be seen that a source on a track upslope of R, such as P_1, generates shorter travel times than one on a path downslope from R, such as P_2, by hundreds of ms. On path P_3, T_5 is larger than $\overline{T}_5$ ($\alpha=0$) initially, but intersects $\overline{T}_5$ at CPA and becomes less than the unperturbed travel time as S moves upslope from R. On the diagonal path, P_4, travel times are greater than all other paths initially, become less than those on path P_3 after intersection with that path, and then approach the $\alpha = 0$ result as S approaches the y-axis. We note that on the y-axis both T_5 and $\overline{T}_5$ should be equal.

The variation of travel time from the horizontal bottom state is more easily seen in Fig. 4 where we present level curves of the change in travel time, ΔT_5, given by Eq. (10d). We observe that $\Delta T_5 > 0$, or $T_5 > \overline{T}_5$, when S is downslope from R (upslope propagation), as expected. Besides the casual observation that $|\Delta T_5|$ increases with range, we see clearly from Fig. 4 that ΔT_5 changes most rapidly when progressing directly upslope along the x-axis. Near R, ΔT_5 changes as much as 50 ms per km when propagating upslope. Thus,

bottom inclination strongly influences travel time, the magnitude of this influence being determined by the relative bearing of S from R.

Geometric spreading loss L_N, for a ray with N bottom reflections and for σ_S and σ_R specified, can be derived from the equation[29]

$$L_N = \left| \frac{\sin \theta_{RN}}{\cos \Theta_{SN}} \left(\frac{\partial x}{\partial \Theta_{SN}} \frac{\partial y}{\partial \phi_{SN}} - \frac{\partial x}{\partial \phi_{SN}} \frac{\partial y}{\partial \Theta_{SN}} \right) \right| \quad , \tag{11a}$$

where the partial derivatives are evaluated at $x = y = 0$, and where

$$x = R \sin \beta - \sum_{0}^{N} L_{kN} \sin \phi_{kN} \tag{11b}$$

and

$$y = R \cos \beta - \sum_{0}^{N} L_{kN} \cos \phi_{kN} \; . \tag{11c}$$

Performing the operations indicated in Eq. (11a) on Eqs. (11b) and (11c), and making substitutions from Eqs. (1)-(5) and (9), we find that, to lowest order terms in α, spreading loss is approximately the square of arc length:

$$L_N \stackrel{\bullet}{=} S_N^2 = \left[cT_N \right]^2 \; . \tag{11d}$$

This equation shows that spreading loss varies as the square of travel time. Therefore, at fixed R, bottom slope causes L_N to be larger for signals transmitted upslope than for signals propagated downslope, as was seen for travel time. Although both bottom inclination and bearing of S from R affect L_N, the variations from the horizontal bottom result are less than 2 dB for typical bottom parameters.

In contrast to spreading loss, bottom loss is known to be particularly significant in shallow water propagation.[24] Thus, bottom slope can be expected to have an impact on transmission loss, $-20 \log_{10} A_N$, where

$$A_N = \prod_{1}^{N} \beta_{kN} L_N^{-1/2} \tag{12}$$

is amplitude and δ_{kN} is the reflection coefficient at bottom bounce k of a ray with N bottom reflections (and σ_S, σ_R specified). We calculate δ_{kN} using a Mackenzie bottom model and our previously developed geometric approximations for Θ_{kN} and ϕ_{kN}. For numerical examples, the parameters used are typical of a sand bottom, so that we take bottom-to-water sound speed ratio to be 1.1658, bottom-to-water density ratio to be 1.9522, and an attenuation parameter of 0.0158.[23] Other bottom parameter values have been shown to generate similar acoustical results.

Level curves of per-ray transmission loss appear in Fig. 5, again for surfaced source and receiver and N = 5. We note that the loss drops as S-R range increases to about 6 km, and then increases with R, although spreading loss increases monotonically with R. This transmission loss behavior is attributed to the bottom loss model, in which the steep angles of incidence at relatively short ranges cause much greater bottom loss than that due to spreading. As range increases, however, the angle of incidence of a ray decreases, causing bottom loss to decrease while spreading loss increases. The transmission loss ultimately increases with range, when spreading loss becomes dominant over bottom loss. This is indicated by the dashed 81 dB level curve shown near the top of Fig. 5. Rays with smaller N exhibit this change in dominance at shorter ranges. The increasing loss with small range values is a consequence of any bottom reflection model which displays monotonically increasing loss with increasing ray angle. For example, the Rayleigh[3] and Mackenzie[23] models both possess such a characteristic.

The deviation from circles of the level curves of Fig. 5 is an influence of bottom inclination. For downslope propagation (S upslope from R), the ray angle of incidence at the bottom becomes closer to grazing with each successive bottom reflection, the rapidity of approach to grazing depending on

both α and S bearing β. For β near 0 and $\pm\pi$ radians, the angles Θ_{kN} (and ϕ_{kN}) exhibit minimum (and maximum) deviation from their horizontal-bottom values. We observe that the transition from bottom loss dominance to spreading loss dominance occurs at shorter ranges for β near 0 or $\pm\pi$, as indicated by the closeness of contours. For example, there is a 10 dB change in transmission loss between 4 and 5 km range here, contrasted with a 6 dB change when $\beta = \pm \pi/2$ rad. Upslope propagation (S downslope from R) similarly exhibits strong dependence on α and β through the bottom-loss model, with the primary distinction that the steepness of a ray tangent now increases with each bottom reflection. This causes the gradient of transmission loss to be smaller in magnitude when propagating upslope compared to downslope. Thus, for a given range, transmission loss for upslope propagation exceeds that for downslope propagation. Qualitatively similar level curves of transmission loss for longer range sound transmissions, obtained using normal mode theory, have been calculated.[10]

The variation of transmission loss as S assumes successive positions on specified paths is shown in Fig. 6. The paths P_1 through P_4 appear in Fig. 5 and are the same as on Fig. 2, with each having a CPA of 5 km. The dashed curve in Fig. 6 is the loss for a horizontal bottom ($\alpha=0$) at depth d_R, for a linear path with a CPA of 5 km. The characteristic dominance of bottom loss over spreading loss at short ranges is easily seen in this broken curve. Path P_1 is an upslope track (downslope propagation) mainly lying in a region dominated by spreading loss, since bottom loss influence dominates in an interval of about 2 km on either side of CPA. We note that transmission loss on P_1 is less than on the same path when $\alpha = 0$. The downslope image of P_1 is P_2, which lies in a region dominated by bottom influence. The preeminence of the effect of altitudinal ray angle Θ_{kN} is seen in the rapid increase of loss

as β approaches $\pi/2$ at CPA. Overall, the sloping bottom causes an increase in transmission loss and a broadness of the region of bottom loss domination. Path P_3 is directly upslope, with minimum transmission loss occurring for downslope propagation. That part of P_3 in which bottom loss dominates, from its start to about 2 km beyond CPA, also shows the strong influence of bottom inclination in changing the spatial variation of transmission loss from the dashed curve. The diagonal trajectory is primarily a bottom loss dominated path, with spreading loss determining the quality of variation only in the last one km. In summary, we see here that a sloping bottom intensifies the variations in transmission loss for paths lying primarily in a region of bottom loss predominance, as for P_2 through P_4, and reduces variations when spreading loss dominates, as for P_1.

We illustrate the influence of the sloping bottom by displaying relative per-ray transmission loss, $-20 \log_{10} (A_5/\overline{A_5})$, as level curves on a spatial grid 14 km square with R at the origin (see Fig. 7). The interval between adjacent level curves is 2 dB in this figure. When propagating downslope (S upslope), the bottom angle causes an increase in signal strength when compared to a horizontal bottom. The converse is true when signals are propagated upslope. The strong influence of bottom inclination is seen from a total variation in transmission loss of more than 24 dB over the figure. Regions of small deviation from the horizontal bottom case are caused by two different mechanisms. First, near the receiver, bottom loss dominates because of steep altitudinal ray angles, and is essentially the same in both the unperturbed ($\alpha=0$) and perturbed cases. Second, at longer ranges, there is dominance of spreading loss, which has only small deviations, as discussed earlier. The absence of an effect of source bearing is seen near the y-axis, where little

variation in Θ_{kN} occurs to produce changes in bottom loss. In the regions of bottom loss dominance, however, the influence of β on ray angles is expressed by more closely spaced level curves, as seen for $|\beta|$ approaching $\pi/2$. Equations (9) show that altitudinal angles θ_{kN} experience relatively large change from $\overline{\Theta}_N$, while azimuthal angles ϕ_{kN} vary only slightly from β, when $|\beta|$ is near $\pi/2$. The conspicuous asymmetry of the level curves is caused by bottom loss effects and the manner of bottom loss change as discussed before. Thus, variation of θ_{kN} with β is the primary cause of the large changes in per-ray transmission loss for propagation over a sloping bottom in regions of bottom loss dominance.

Before discussing total field, a brief overview of the relationship among its constituents is appropriate. In Table I, we display the relative magnitude $\overline{A}_N/\overline{A}_1$ and the relative per-ray transmission loss $-20 \log_{10} (A_N/\overline{A}_N)$ for the first nine ray arrivals at R when S is located upslope at $(R, \beta) = (5, -75°)$ and downslope at $(5, +75°)$. For these values of β, S lies in a region where bottom loss dominates spreading loss. As N increases, the relative amplitude of an unperturbed-state ray compared to that of the strongest $N = 1$ ray decreases, while $-20 \log_{10} (A_N/\overline{A}_N)$ becomes significant. This shows that large changes in relative transmission loss are associated with ray components of less significant magnitude in the total acoustic field. We see little variation in per-ray transmission loss for $N \leq 3$; however, for upslope propagation (S downslope), the difference in bottom loss becomes substantial at $N = 4$. Signals propagating downslope show significant deviation from the horizontal-bottom sound channel for $N \geq 5$. The quantitative differences with N between upslope and downslope propagation arise from the sensitivity of the Mackenzie bottom-loss model to incident ray angle at the bottom.

We now briefly consider bottom slope effect on incoherent total-field amplitude. Specifically, we examine the range R to level curves of transmission loss, $-10 \log_{10} A^2$, where

$$A^2 = \sum_N A_N^2 , \tag{13a}$$

in which A_N is given by Eq. (12). Similarly, we consider the constant range $\overline{R}$ to level curves of $-10 \log_{10} \overline{A}^2$, where

$$\overline{A}^2 = \sum_N \overline{A}_N^2 \tag{13b}$$

is the corresponding amplitude-squared for a horizontal bottom of depth d_R. We use the same parameter values and S-R placement as before, and consider level curve values of 65, 68, and 71 dB. For each fixed transmission loss value, we calculated the percentage change in range, $100 \, (R-\overline{R})/\overline{R}$. The results appear in Fig. 8 as a function of bearing angle β. We observe that the range to each level curve is greater for downslope propagation ($\beta < 0$) and shorter for upslope propagation, so that downslope propagation exhibits a larger percentage variation. For the solid curve (71 dB), $\overline{R}$ has the constant value 6.8 km, while $\overline{R} = 3.8$ km for 68 dB, and $\overline{R} = 1.7$ km for 65 dB. Percent changes in range varies a total of more than 40% as β assumes all possible values for the 71 dB contour, reflecting the influence of bottom inclination.

The primary cause of this variation is the change in ray angles at bottom reflection points with, for downslope propagation (i.e., $\beta < 0$), the rays starting more steeply than for a horizontal bottom and becoming shallower with each bottom bounce. Table I shows that strong rays have small N, whereas Eqs. (9) imply that the strong rays have least change in geometry from the horizontal bottom rays. Consequently, strong rays exhibit transmission loss

close to unperturbed rays. For both the 71 dB and 68 dB contours, the rays for

$N = 1, 2$, and 3 dominate the total field; however, other rays contribute at

least through $N = 6$. The lessening of the altitudinal angle at each successive

bottom reflection causes range to the fixed transmission loss curve to

increase. Percent range variation for upslope propagation (i.e., $\beta > 0$) is

explained similarly. Rays with multiple bottom bounces are steeper at

successive bottom reflections. This increased loss tends to shorten the range

to level curves of transmission loss. At short range (i.e., the 65 dB

contour), both the rays over a sloping bottom and those over a horizontal one

are so steep that there is little variation in bottom loss between them. The

strong effect of β seen in each curve is predicted by its effect on each ray

from Eqs. (9).

III. COMBINED SLOPE AND FRONTAL EFFECTS

Oceanic fronts can occur in the continental margin and in other shallow-

water regions.[30,31] Such fronts have been modelled numerically (see, for

example, Ref. 4) and studied analytically for a horizontal bottom.[25] A

sloping bottom induces significant variation in acoustical quantities as shown

in Sec. II, while Ref. 25 demonstrates frontally induced variations in a

horizontal bottom sound channel. We examine here the influence of a plane

bottom which slopes away from shore on sound transmission through a front in

shallow water.

We use a model which defines the front as a vertical plane separating

water masses of constant, but different, sound speed on either of its sides.

Our simple model includes uniform but different horizontal currents on both

sides of the front, as well. The front is oriented parallel to the shore,

and we place S and R on opposite sides of it. As in previous sections, the

sound speed at R is c, while the source-side sound speed c_S is related to c by

$$c_S = c + \Delta c. \qquad (14a)$$

It is convenient to introduce the dimensionless sound speed jump Δ, defined by

$$\Delta = \Delta c/c . \qquad (14b)$$

Typically, the along front currents in shallow water vary in magnitude between 2 and 16 cms^{-1}, but magnitudes exceeding 30 cms^{-1} are not uncommon.[31] The coordinate system established in Sec. I and depicted in Fig. 1 is maintained here, and the equation for the frontal plane is $x = x_F$. The distance d_F from R to the front, along the source-receiver line, is

$$d_F = -x_F \csc \beta , \qquad (14c)$$

where $|\beta|$ cannot be zero or π since we permit neither S nor R to lie in the frontal plane. The inclination angle β^* of the frontal plane to the S-R line is related to the source bearing by

$$\beta^* = H(\beta)\pi - \beta . \qquad (14d)$$

The quantities x_F, d_F, and β^* are shown in the inset of Fig. 9.

We extend the notation of Sec. I to indicate the side of the front (source or receiver) on which a quantity lies, by appending an S or R subscript. For example, if the front intersects a ray path between the last bottom reflection and R, the altitudinal angle is Θ_{NNS} before reaching the front, and Θ_{NNR} after the ray passes through the front. However, the altitudinal angle Θ_{RN} of the ray tangent incident at R is an example of a

quantity whose location is assumed known (on the receiver side of the front), so that no additional subscript is written.

We determine ray geometry for fixed S and R by tracing a ray forward from S through the front to R, assuming that neither a surface nor bottom reflection point occurs at the plane of the front. For any given ray with N bottom reflections, we take the front to lie in lobe n of that ray path. Ray tangents on either side of the front are as described in Sec. I:

$$\underset{\sim}{\Lambda}_{kNS} = \begin{pmatrix} \cos 2k\alpha \, \cos \Theta_{oNS} \sin \phi_{oNS} - \sin \Theta_{oNS} \sin 2k\alpha \\ -\cos \Theta_{oNS} \cos \phi_{oNS} \\ \sin \Theta_{oNS} \cos 2k\alpha + \cos \Theta_{oNS} \sin \phi_{oNS} \sin 2k\alpha \end{pmatrix} , \quad 0 \leq k \leq n, \tag{15a}$$

and

$$\underset{\sim}{\Lambda}_{kNR} = \begin{pmatrix} \cos \Theta_{NNR} \sin \phi_{NNR} \cos 2(N-k)\alpha + \sin \Theta_{NNR} \sin 2(N-k)\alpha \\ -\cos \Theta_{NNR} \cos \phi_{NNR} \\ \sin \Theta_{NNR} \cos 2(N-k)\alpha - \cos \Theta_{NNR} \sin \phi_{NNR} \sin 2(N-k)\alpha \end{pmatrix} , \quad n \leq k \leq N. \tag{15b}$$

Two range relations are

$$(R-d_F) \sin \beta = \sum_{0}^{n} L_{kNS} \sin \phi_{kNS} \tag{16a}$$

and

$$d_F \sin \beta = \sum_{n}^{N} L_{kNR} \sin \phi_{kNR} , \tag{16b}$$

where L_{nNS} is the projection on the xy-plane of that portion of the ray path in lobe n on the source side of the front, and similarly for L_{nNR} on the receiver side of the front.

The effect of the front on a ray is to bend it, the refraction relation being[26]

$$(1+\Delta)\underline{\Lambda}_{nNR} = \underline{\Lambda}_{nNS} - \Gamma\underline{M}_F , \tag{17a}$$

where

$$\Gamma = \left[(1+\Delta)^2 - 1 + (\underline{\Lambda}_{nNS}\cdot\underline{M}_F)^2\right]^{1/2} - \underline{\Lambda}_{nNS}\cdot\underline{M}_F , \tag{17b}$$

and $\underline{M}_F$ is the unit normal to the plane of the front on the receiver side. As in Sec. I, we can relate horizontal distances, water depths, and angles by using Eqs. (6) on either side of the front. For example, Eq. (6b) when applied on the source side of the front gives L_{kNS} for $1 \leq k \leq n$ as a function of h_{kNS}, Θ_{kNS}, ϕ_{kNS}, and α. We insure continuity of the ray path by matching the ray traced backward from R to the ray traced forward from S using the refraction relation Eq. (17a). To trace from R, we need one additional relation,

$$h_{NNR} = \left(d_R \tan \Theta_{NNR} + \sigma_R h_R \tan \alpha \sin \phi_{NNR}\right)$$
$$\times \left(\tan \Theta_{NNR} - \tan \alpha \sin \phi_{NNR}\right)^{-1} . \tag{18}$$

The equations derived from Eqs. (6) and Eqs. (15)-(18) form a non-linear deterministic system for Θ_{oNS}, Θ_{NNR}, ϕ_{oNS}, and ϕ_{NNR}.

Next, we write

$$\Theta_{kNS} = \overline{\Theta}_N + \varepsilon_{kNS} \quad , \quad 0 \leq k \leq n \quad , \tag{19a}$$

$$\Theta_{kNR} = \overline{\Theta}_N + \varepsilon_{kNR} \quad , \quad n \leq k \leq N. \tag{19b}$$

$$\phi_{kNS} = \beta + \chi_{kNS} \quad , \quad 0 \leq k \leq n , \tag{19c}$$

and

$$\phi_{kNR} = \beta + \chi_{kNR} \quad , \quad n \leq k \leq N , \tag{19d}$$

23

where the overbar on Θ is an altitudinal angle of the corresponding ray when no front and no bottom slope are present. Thus, the ε and χ terms represent corrections to altitudinal and azimuthal angles which arise from a sloping bottom and/or the presence of a front. We assume that the angle changes from $\overline{\Theta}_N$ and β are small relative to unity so that we can approximate the deviations by perturbation methods. Further, the orders of magnitude of the sloping-bottom parameter α and the dimensionless frontal parameters Δ and signed Mach numbers $\mu_S = \pm\,|v_S|/c$ and $\mu_R = \pm\,|v_R|/c$ must be specified, so that terms of the correct degree are kept in expansions. In particular, for moderate fronts, $\Delta = O(10^{-2})$,[30] and for α between $1/2°$ and $1°$, α in radians satisfies $\Delta = \theta(\alpha)$. However, $|\mu_S|$ and $|\mu_R|$ are typically $O(10^{-4})$[31] so that Mach numbers may be ignored when only first degree terms in Δ and α are kept in our expansions.

Under these conditions, we approximate Λ_{kNS} and Λ_{kNR} from Eqs. (15). Substituting the results into Eqs. (17) gives an approximation for Γ, and a relation between Λ_{nNR} and Λ_{nNS} to linear terms in α and Δ. These results are extended further by additional approximations from Eqs. (19), assuming that linear terms in α, Δ, ε_{oNS}, ε_{NNR}, χ_{oNS}, and χ_{NNR} are actually of the same order. We use the ratios of the x and y components, and of the z and y components, from Eq. (17a), to express angle changes in terms of α, Δ, and angle change at S and R. Substituting the results into Eqs. (6) and (18) and then into Eqs. (16), and retaining linear terms in α and Δ, we find approximations of ε_{oNS}, ε_{NNR}, χ_{oNS}, and χ_{NNR} in terms of α and Δ. Under the conditions that rays are neither very steep nor close to grazing upon incidence to the front ($\Delta\,\sec^2\theta_N\,\csc^2\beta^* \ll 1$),[25] nor close to grazing on bottom incidence, we have

$$\epsilon_{oNS} \doteq -\alpha \left\{ 2N(N+\sigma\hat{h}_R)\hat{R}^{-1} \sin \beta \cos \overline{\theta}_N \sin \overline{\theta}_N \right\}$$

$$+ \Delta \, \hat{d}_F\hat{R}^{-1} \tan \overline{\theta}_N \quad , \tag{20a}$$

$$\epsilon_{NNR} \doteq -\alpha \left\{ 2N(N+\sigma\hat{h}_R)\hat{R}^{-1} \sin \beta \cos \overline{\theta}_N \sin \overline{\theta}_N \right.$$

$$\left. - 2N \sin \beta \right\} - \Delta(1-\hat{d}_F\hat{R}^{-1})\tan \overline{\theta}_N \quad , \tag{20b}$$

$$X_{oNS} \doteq \alpha \; 2N(N+\sigma_R\hat{h}_R)\hat{R}^{-1} \cos \beta$$

$$+ \Delta \, \hat{d}_F\hat{R}^{-1} \sec^2 \overline{\theta}_N \cot \beta^\star \quad , \tag{20c}$$

and

$$X_{NNR} \doteq \alpha \left[2N(N+\sigma_R\hat{h}_R)\hat{R}^{-1} \cos \beta - 2N \cos \beta \tan \overline{\theta}_N \right]$$

$$- \Delta \, (1-\hat{d}_F\hat{R}^{-1})\sec^2 \overline{\theta}_N \cot \beta^\star \quad , \tag{20d}$$

where $\hat{d}_F = d_F/d_?$ is a dimensionless distance from $\hat{R}$ to the front. Recalling that θ_{SN} and θ_{RN} are always on the source and receiver sides of the front, respectively, Eqs. (1) complete the geometric approximations. The results given in Eqs. (20) reduce to those in Sec. I when $\Delta = 0$ and reduce to those in Ref. 25 [for $\mu_R = \mu_S = 0$] when $\alpha = 0$.

We calculate travel time from

$$T_N = c^{-1} \sum_{S \; 0}^{n} L_{kNS} \sec \theta_{kNS} + c^{-1} \sum_{n}^{N} L_{kNR} \sec \theta_{kNR} \quad , \tag{21a}$$

in which the first (and second) term is the travel time from S to the front (and from the front to R). Using the approximations of Eqs. (20) in Eq. (21a) and expanding to linear terms in α and Δ gives

$$T_N \doteq \overline{T}_N \left\{ 1 + 2N\alpha \sin\beta \left[N+\sigma_R\hat{h}_R\right]\hat{R} \right.$$
$$\times \left[\hat{R}^2 + (2N+\sigma_S\hat{h}_S+\sigma_R\hat{h}_R)^2\right]^{-1}$$
$$\left. - (1-\hat{d}_F\hat{R}^{-1})\Delta \right\} \quad , \tag{21b}$$

where $\overline{T}_N$ is given by Eq. (10c) and is the travel time in the absence of both the front and the sloping bottom.

To illustrate the influence of a sloping bottom on propagation through a front, we calculate T_5 with $c = 1500$ ms^{-1}, $\Delta c = 20$ ms^{-1}, $x_F = -2$ km, $d_R = 300$ m, and source and receiver on the surface. The value of Δc is typical of the Slope Front in the North Atlantic.[32] The results for travel time $\Delta T_5 = T_5 - \overline{T}_5$ are shown in Fig. 9, for three values of bottom slope α, as S occupies successive positions along two paths, each with a CPA 5 km downslope from R. The solid path P_1 is parallel to the shore, whereas the dashed path P_2 tracks diagonally upslope. The curves for $\alpha = 0$ represent the influence of the front in a horizontal bottom sound channel. Note that on path P_1, the front induces maximum $|\Delta T_5|$ at the beginning (and end) of P_1 where β is closest to π (or zero) and where the relative front location $\hat{d}_F\hat{R}^{-1}$ is smallest. For $\alpha = 0.5°$ the bottom inclination cancels the frontal effect at the ends of the track and increases ΔT_5 by more than 60 ms at CPA over that for $\alpha = 0°$. When $\alpha = 1°$, the bottom angle accounts for more than 140 ms of the value of ΔT_5 at CPA.

For S tracking diagonally upslope on path P_2, symmetry about CPA disappears. At the end of the track when $\alpha = 0°$, ΔT_5 is 20 ms more than its value at the start of the path. For larger α we again see an increasingly strong influence of the sloping bottom. Notice that the sloping bottom exerts a weaker influence near the end of P_2 because β is becoming small, causing the inclination induced travel-time change to be small, as was suggested in Fig. 4. The strongest frontal effect occurs when relative front location $\hat{d}_F \hat{R}^{-1}$ is smallest at the start of P_2, but the inclined bottom effect is large there also, because β is near $\pi/2$. Thus, we see that the peak of ΔT_5 when $\alpha \neq 0$ occurs before CPA because of the asymmetric variation in frontally induced travel time change.

A primary qualitative difference in the behavior of ΔT_5 on the two paths comes from the manner in which the front affects travel time. When $\alpha = 0$, Eq. (21b) predicts the behavior we illustrate. Frontally induced travel time change varies as $\hat{d}_F \hat{R}^{-1}$ and shows symmetric behavior about CPA on P_1, but monotonicity on P_2. The change in ΔT_5 induced by the sloping bottom alone on path P_1 exhibits the same symmetric increase and decrease about the CPA as did the travel-time change caused by the front. These effects are additive when $\alpha \neq 0$ and produce curves with the same general properties. In contrast, the variation in ΔT_5 caused by the sloping bottom alone is asymmetric about the CPA and has an increasing and then decreasing behavior. When $\alpha \neq 0$, the asymmetry is more pronounced, with the dominant influence of the sloping bottom determining the illustrated behavior. The influence of the front on ΔT_5 is more pronounced for $\alpha = 0.5°$ than for $\alpha = 1°$ because the relative magnitude of frontally induced ΔT_5 ($\alpha=0$) compared to that caused by the bottom angle is less when $\alpha = 1°$.

Downslope propagation is illustrated by placing S upslope from R, and adjusting the frontal parameter Δc to correspond to warmer water offshore from the front. We display ΔT_5 for the same three values of α on two paths upslope from R

in Fig. 10, with $c = 1520$ ms^{-1}, $\Delta c = -20$ ms^{-1}, $x_F = 2$ km, and other parameters as in Fig. 9. The paths are similar to those previously described, except that P_1 is parallel to the shore with CPA 5 km upslope from R. Path P_2 again tracks diagonally upslope with a 5 km CPA to R. Since we are now transmitting from cold to warm water ($\Delta c < 0$), the front alone ($\alpha = 0$) causes ΔT_5 to be positive. However, as seen in Fig. 4, the sloping bottom generates negative ΔT_5 for downslope propagation. The effect of the sloping bottom on the frontal influence for downslope propagation is analogous to that for upslope propagation. Comparison of Figs. 9 and 10 reveals that the concavity reversal from upslope to downslope propagation is a result of Δc changing sign, with a corresponding change in the sloping bottom travel time effect. The difference in locations of peak (minimum) ΔT_5 when $\alpha \neq 0$ on path P_2 is a result of the different locations of peak (minimum) ΔT_5 caused by the sloping bottom, as suggested in Fig. 4. Traversing path P_2 in Fig. 10 in an opposite direction causes the relative extrema of ΔT_5 to occur slightly before CPA as in Fig. 9. The strong travel time influence, on signals transmitted through a shallow water front, of the bottom inclination (approximately 150 ms shown) is qualitatively similar whether transmitting upslope or downslope.

As discussed in Sec. II and in Ref. 24, the sloping bottom exerts a much stronger effect on transmission loss than that produced by a front. Consequently, we will not consider those combined effects here. Results of this section have shown that bottom inclination has a profound effect on travel time changes induced by a moderate strength front in shallow water.

IV. SUMMARY

Effects of a sloping ocean bottom on three-dimensional per-ray arrivals at a receiving point, and on incoherent total-field transmission loss, are examined. The ocean medium is usually modelled as isospeed, although an ocean

28

with two distinct sound speeds is used to examine propagation through a front on the continental shelf and parallel to the shore. The sound source and receiver are at arbitrary depths, and their relationship to the sloping bottom is arbitrary. Short range propagation for source-receiver paths having both upslope and downslope components are investigated. New approximations for ray geometry over the sloping bottom are found by perturbing from the basic state in which the bottom is horizontal with water depth of the receiver.

Principal features of variations induced by the sloping bottom are investigated. An approximation to change in per-ray travel time is derived which demonstrates dependence on source-receiver location over the slope and on bottom angle. In numerical examples, it is shown that the travel time change for a ray with five bottom reflections is approximately $\pm$ 200 ms at a range of about 5 km, where the sign depends upon source-receiver orientation.

One of the new results from our formulas is that although the sloping bottom causes an insignificant change in spreading loss, it induces significant changes in per-ray transmission loss through bottom loss effects. This fact is illustrated for a Mackenzie bottom, but it would hold for many other bottom models. Upslope propagation is shown to experience greater transmission loss than downslope propagation. In comparison to a flat bottomed sound channel, a bottom inclination angle of 2° induces a decrease (or increase) of approximately 10 dB (or 14 dB) when propagating downslope (or upslope) over a range of about 5 km.

The range from receiver to level curves of total-field transmission loss is examined as a percentage change from the range to corresponding level curves in a sound channel with horizontal bottom. It is found in examples that the range varies by over $\pm$ 20%, the sign depending upon down or upslope propagation.

Finally, we add to the sloping channel a model of a moderate strength shallow water front, parallel to the shoreline, and characterized by different sound speeds on either side of a vertical plane. Geometric and travel time approximations are developed when bottom slope and relative change in sound speed across the front are of the same magnitude. We find that bottom inclination induces significant variations in the travel time change predicted by the frontal model with a flat bottom. Indeed, numerical examples are presented in which bottom slope induces a 400% increase in travel time change when a signal is propagated upslope over a range of 5 km.

[1] G. Neumann and W. J. Pierson, Jr., Principles of Physical Oceanography, (Prentice-Hall, Englewood Cliffs, 1966), pp. 14-33.

[2] N. S. Ageyev, I. B. Andreyeva, V. I. Volovov, Yu. Yu. Zhitkousky, S. D. Chupov, and R. F. Shvacho, in Akustika Okeana, ed. by L. M. Brekhovskikh, (USSR Academy of Sciences, Moscow, 1974), pp. 19-32.

[3] C. B. Officer, Introduction to the Theory of Sound Transmission, (McGraw-Hill, New York, 1958), pp. 74-116.

[4] T. Akal, in Bottom-Interacting Ocean Acoustics, ed. by W. A. Kuperman and F. B. Jensen, (Plenum, New York, 1980), pp. 557-575; M. C. Ferla, G. Dreini, F. B. Jensen, and W. A. Kuperman, ibid., pp. 577-592.

[5] D. E. Weston, Proc. Phys. Soc. (London) 73, 365-384 (1959).

[6] D. E. Weston, Proc. Phys. Soc. (London) 78, 46-52 (1961).

[7] H. Weinberg and R. Burridge, J. Acoust. Soc. Am. 55, 63-79 (1974).

[8] M. J. Jacobson and J. G. Clark, J. Acoust. Soc. Am. 41, 167-176 (1967).

[9] M. J. Jacobson and J. T. Warfield, J. Acoust. Soc. Am. 43, 15-24 (1968).

[10] D. L. Bradley, "The Propagation of Sound in a Wedge Shaped Shallow Water Duct", Ph.D. Thesis, The Catholic Univ. of Am., Washington, D. C. (1970) (unpublished).

[11] C. H. Harrison, J. Acoust. Soc. Am. 62, 1382-1388 (1977).

[12] C. H. Harrison, J. Acoust. Soc. Am. 65, 56-61 (1979).

[13] S. T. McDaniel, J. Acoust. Soc. Am. 58, 1178-1185 (1975).

[14] S. T. McDaniel, J. Acoust. Soc. Am. 72, 177-186 (1980).

[15] F. B. Jensen and W. A. Kuperman, J. Acoust. Soc. Am. 67, 1564-1566 (1980).

[16] A. O. Williams, Jr., J. Acoust. Soc. Am. 67, 177-185 (1980).

[17] A. Kamel and L. B. Felsen, J. Acoust. Soc. Am. 73, 1120-1130 (1983).

[18] A. D. Pierce, J. Acoust. Soc. Am. 74, 1837-1847 (1983).

[19] J. M. Arnold and L. B. Felsen, J. Acoust. Soc. Am. 73, 1105-1119 (1983).

[20] D. S. Ahluwalia and J. B. Keller, in Wave Propagation and Underwater Acoustics, ed. by J. B. Keller and J. S. Papadakis (Springer-Verlag, New York, 1977), Ch. 2.

[21] K. G. Hamilton, W. L. Siegmann, and M. J. Jacobson, J. Acoust. Soc. Am. 66, 1108-1119 (1979).

[22] S. Itzikowitz, M. J. Jacobson, and W. L. Siegmann, J. Acoust. Soc. Am. 74, 1250-1266 (1983).

[23] K. V. Mackenzie, J. Acoust. Soc. Am. 32, 221-231 (1960).

[24] P. H. Rogers, "Onboard Prediction of Propagation Loss in Shallow Water," Naval Research Lab., Washington, D. C., NRL Rep. 8500 (1981).

[25] T. H. Rousseau, W. L. Siegmann, and M. J. Jacobson, "Influence of shallow-water fronts on sound transmission and prediction of frontal parameters", Rensselaer Polytechnic Institute, Troy, NY (in preparation).

[26] M. Herzberger, Modern Geometric Optics, (Interscience, New York, 1958), pp. 3-10.

[27] K. Hoffman and R. Kunze, Linear Algebra, 2nd ed., (Prentice-Hall, Englewood Cliffs, 1971), pp. 87-96, 163.

[28] IMSL Library, Edition 9, (IMSL, Inc., Houston, 1982), pp. ZSCNT-1-ZSCNT-3.

[29] J. T. Warfield and M. J. Jacobson, J. Acoust. Soc. Am. 50, 342-347 (1971).

[30] R. E. Cheney and D. E. Winfrey, "Distribution and classification of ocean fronts", U. S. Naval Oceanogr. Office, Washington, DC, Tech. Note 3700-56-76 (1976).

[31] M. J. Bowman and W. E. Esias, Eds. Oceanic Fronts in Coastal Processes (Springer-Verlag, New York, 1978).

[32] R. W. James and R. E. Cheney, "Physical characteristics of ocean fronts and eddies in the North Atlantic", U. S. Naval Oceanogr. Office, Washington, DC, Tech. Note 3700-59-77 (1977).

TABLE I. Relative amplitude and transmission loss (dB) for first nine
          rays incident on R.   R = 5 km, β = 75° (S downslope),
          β = -75° (S upslope); other parameters as in Fig. 2.

N	$\overline{A}_N/\overline{A}_1$ Rel. Magnitude	$-20\ \log_{10}(A_N/\overline{A}_N)$	
		Upslope	Downslope
1	1.00	− 0.11	+ 0.09
2	0.91	− 0.43	+ 0.26
3	0.80	− 0.55	+ 0.94
4	0.66	− 1.15	+ 8.08
5	0.31	− 4.98	+14.00
6	0.042	−14.96	+ 9.41
7	0.009	−18.77	+ 7.41
8	0.002	−20.39	+ 6.47
9	0.0007	−20.92	+ 5.24

FIGURE LEGENDS

FIG. 1.   (a) Perspective view of typical ray geometry, $N = 3$.

(b) Top view.

FIG. 2.   Level curves of travel time T_5 in seconds, with increments of 0.5 s. $\alpha = 2°$, $c = 1500$ ms^{-1}, $d_R = 300$ m, $h_S = h_R = 0$, $N = 5$.

FIG. 3.   Solid curves: travel time T_5 along paths $P_1 - P_4$ of Fig. 2. Dashed curve: travel time for $\alpha = 0$. Parameters as in Fig. 2.

FIG. 4.   Level curves of travel time change ΔT_5 in milliseconds with increments of 50 ms. Parameters as in Fig. 2.

FIG. 5.   Level curves of per-ray transmission loss in increments of 3 dB. Sand bottom and a Mackenzie bottom loss model. Other parameters as in Fig. 2.

FIG. 6.   Per-ray transmission loss along paths $P_1 - P_4$ of Fig. 5. Dashed curve is $\alpha = 0$. Parameters as in Fig. 5.

FIG. 7.   Level curves of relative per-ray transmission loss, $-20 \log_{10} (A_5/\overline{A_5})$, in increments of 2 dB. Parameters as in Fig. 5.

FIG. 8.   Percent variation in range to level curves of incoherent total-field transmission loss. Loss values are 65, 68, and 71 dB. Parameters as in Fig. 5.

FIG. 9.   Variation of ΔT_5 along paths P_1 and P_2 for three values of α. $c = 1500$ ms^{-1}, $\Delta c = 20$ ms^{-1}, $x_F = -2$ km. Other parameters as in Fig. 2.

FIG. 10. Variation of ΔT_5 along paths P_1 and P_2 for three values of α. $c = 1520$ ms^{-1}, $\Delta c = -20$ ms^{-1}, $x_F = 2$ km. Other parameters as in Fig. 2.

(a) PERSPECTIVE VIEW

(b) TOP VIEW
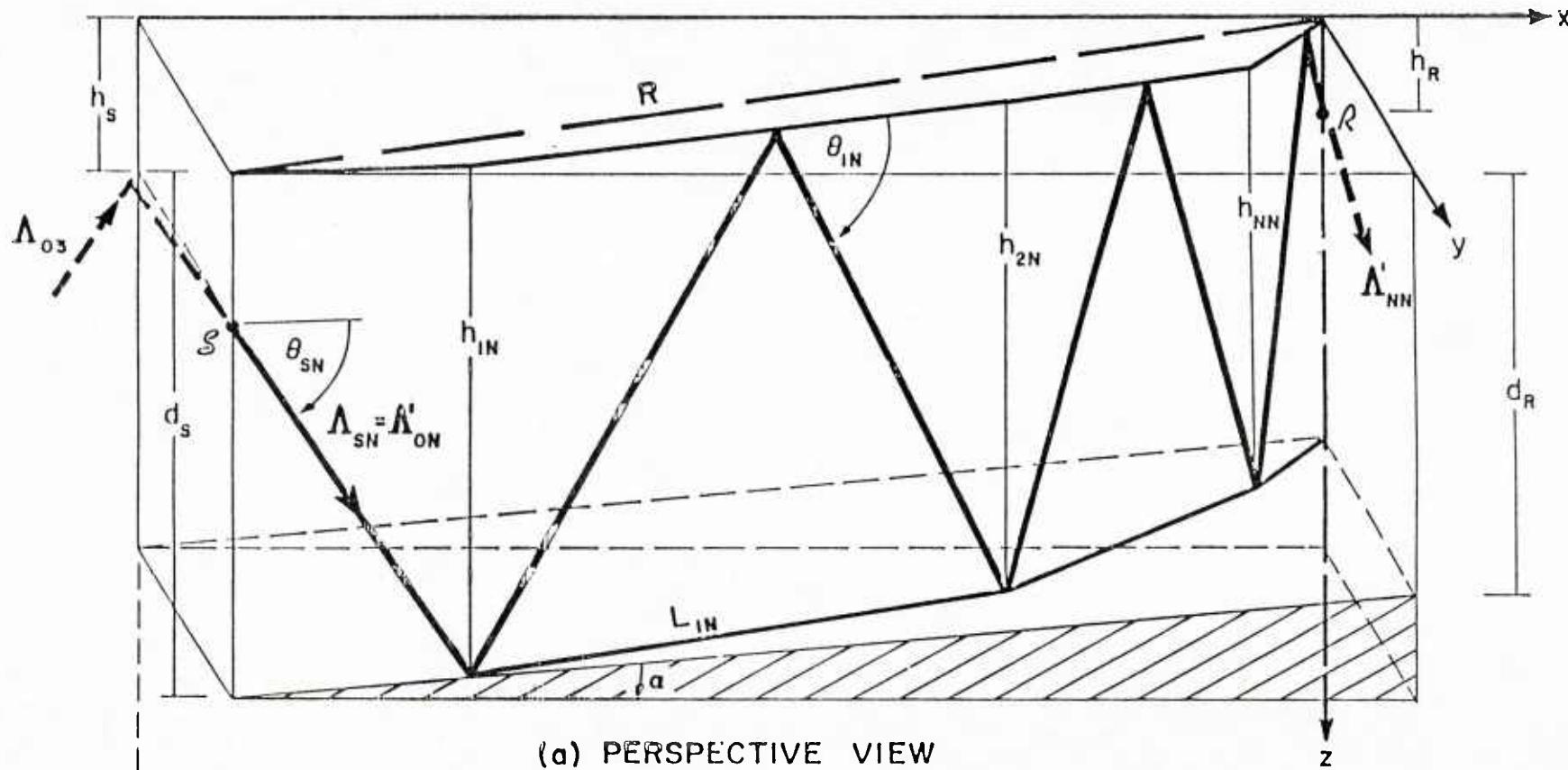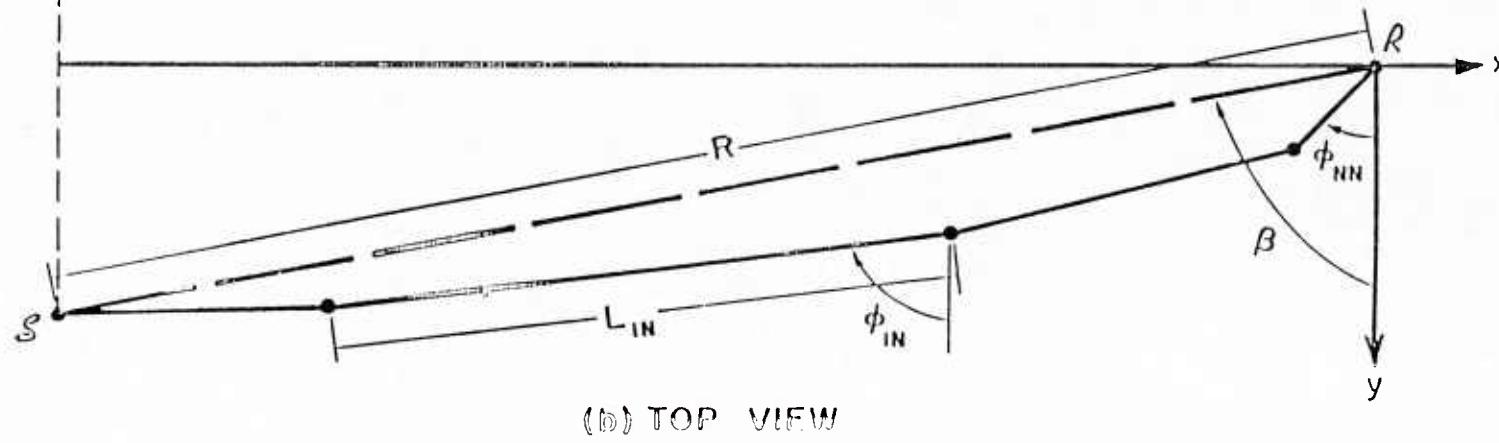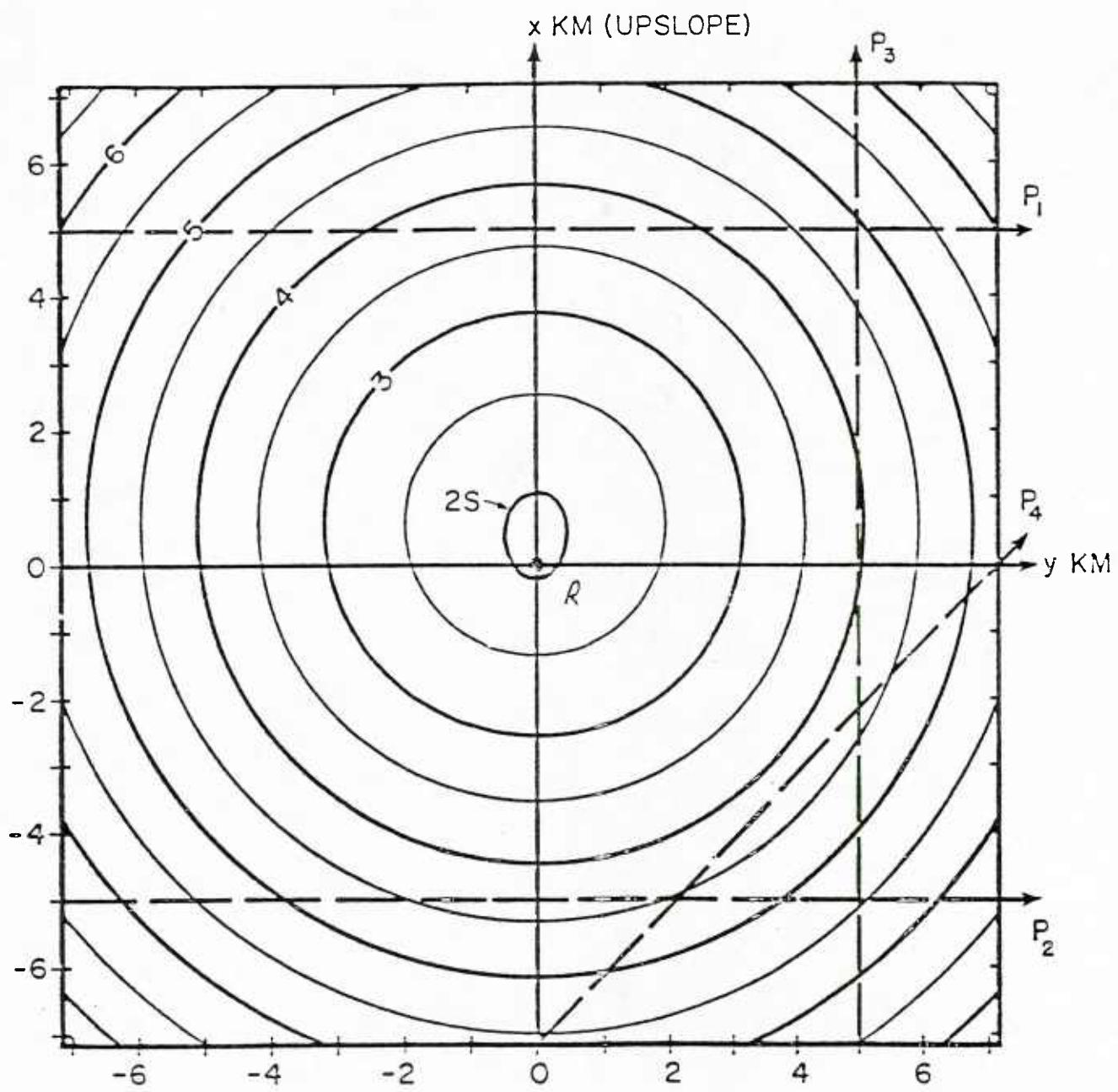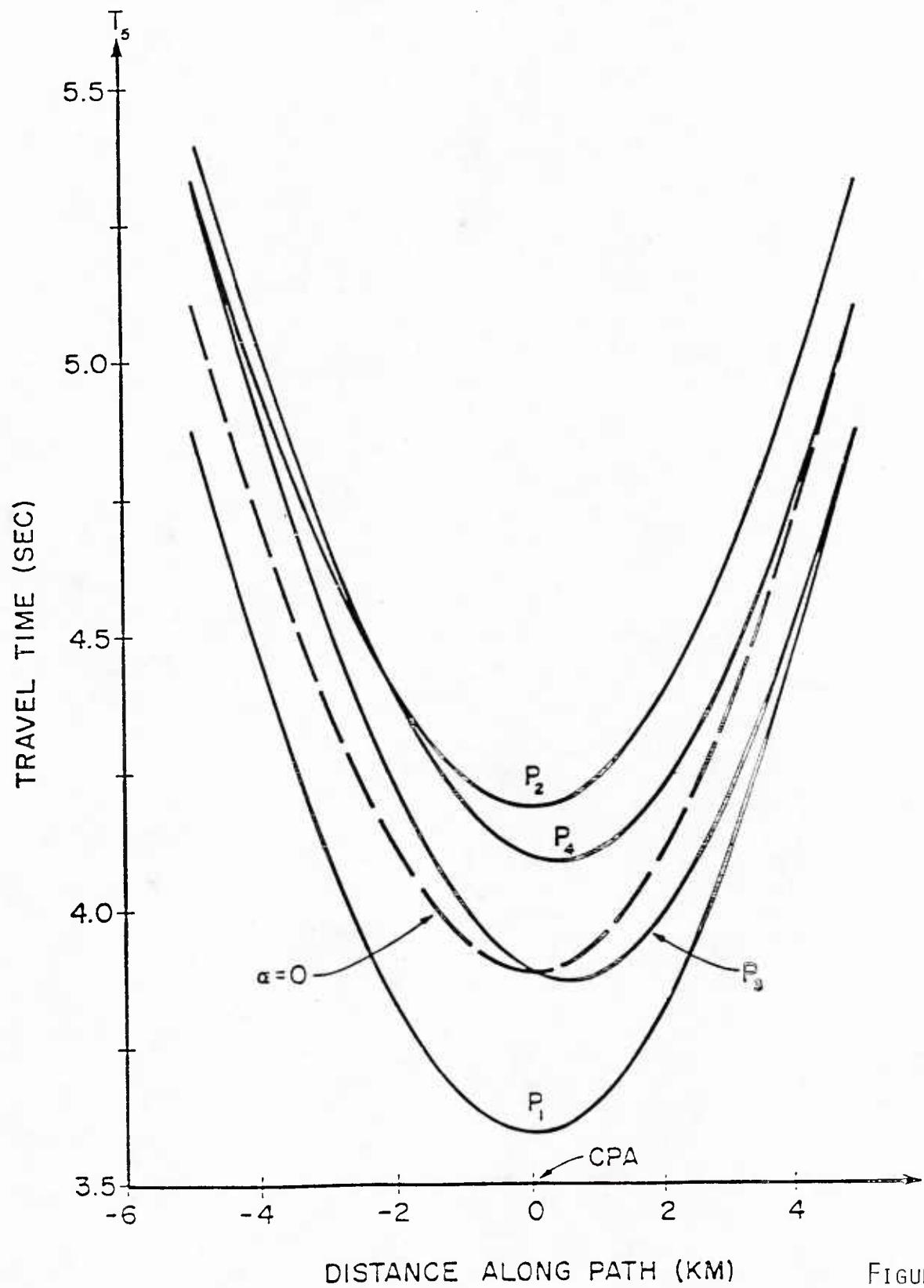
FIGURE 1

FIGURE 2

FIGURE 3
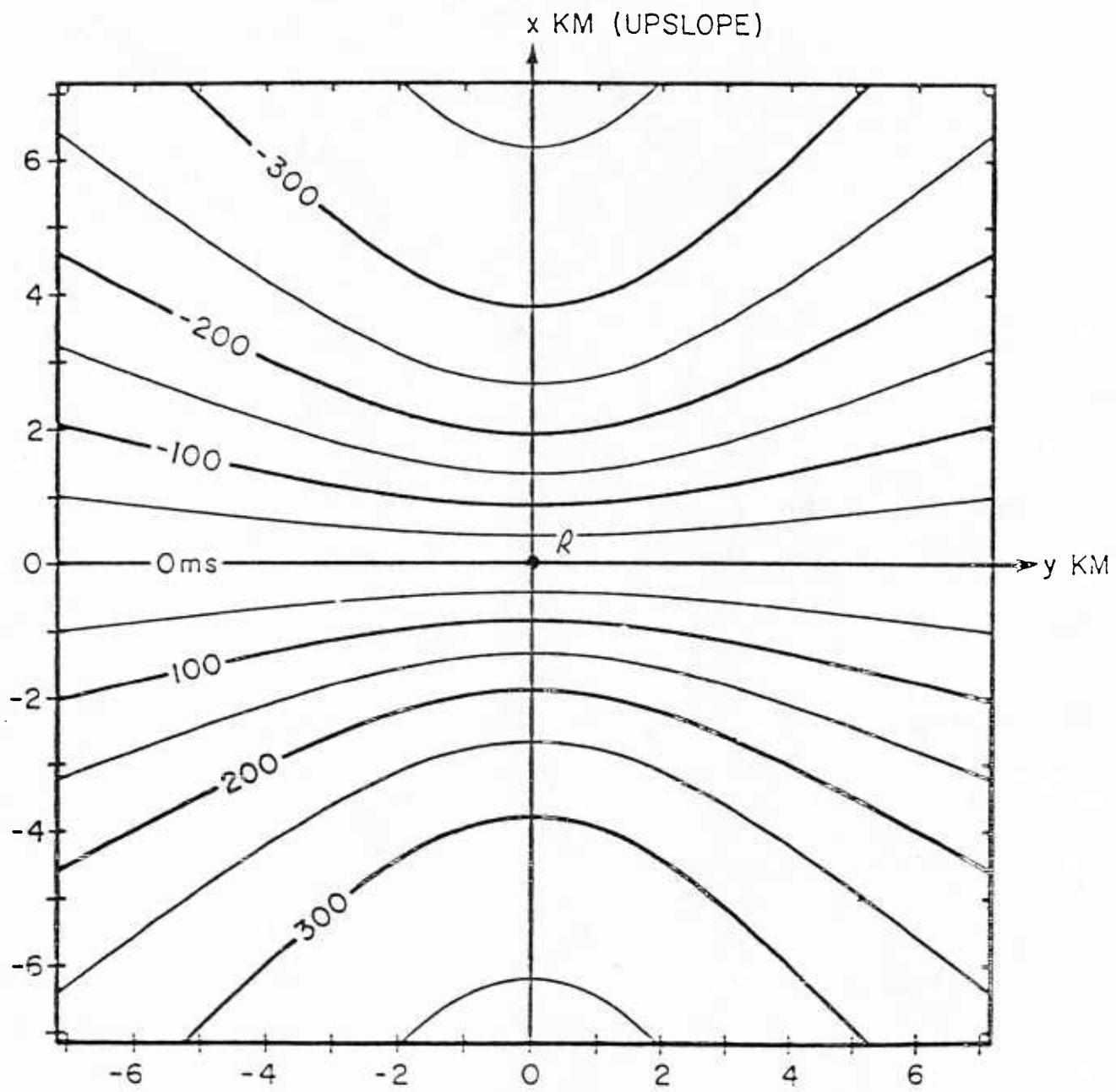
FIGURE 4
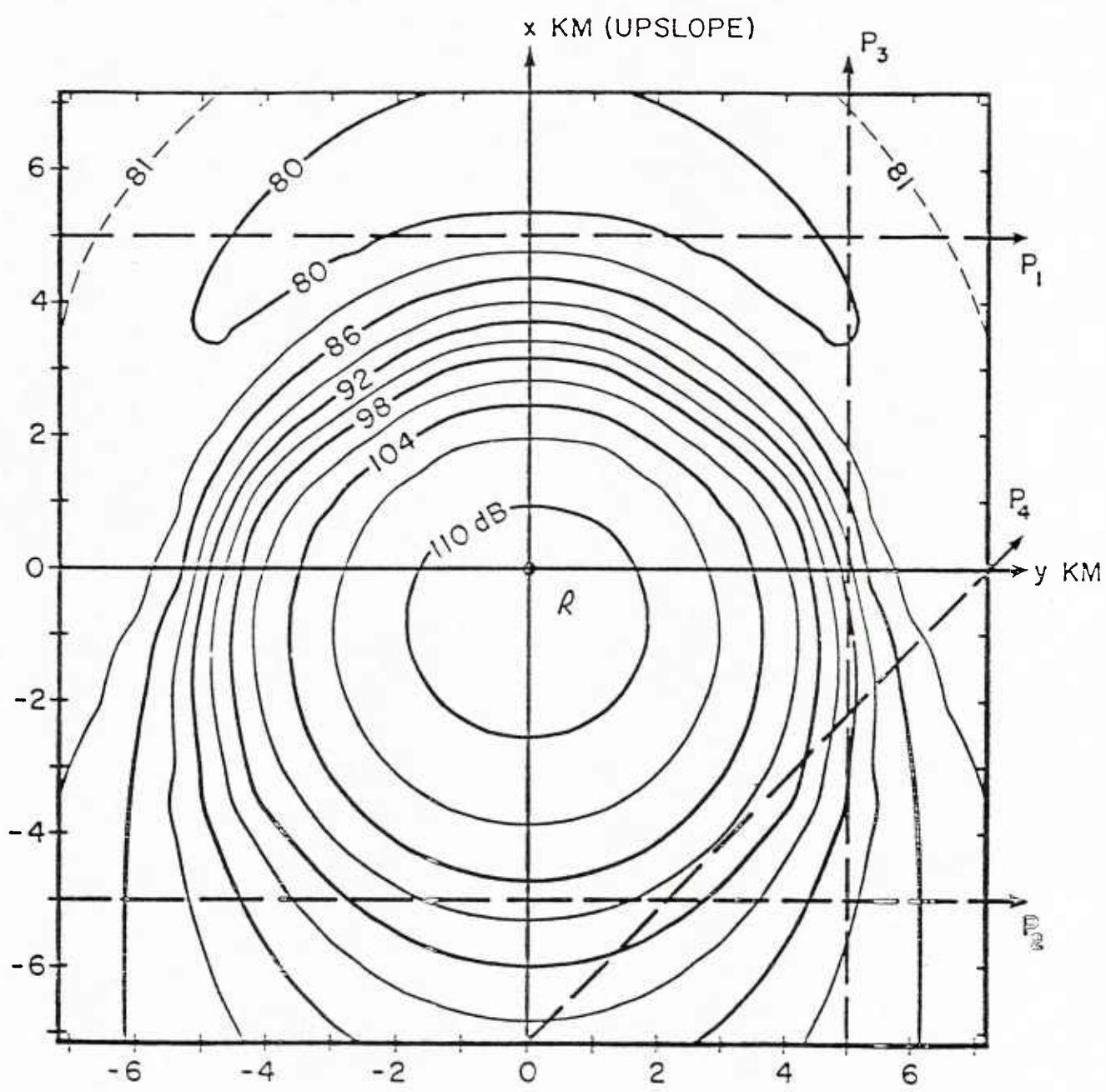
FIGURE 5
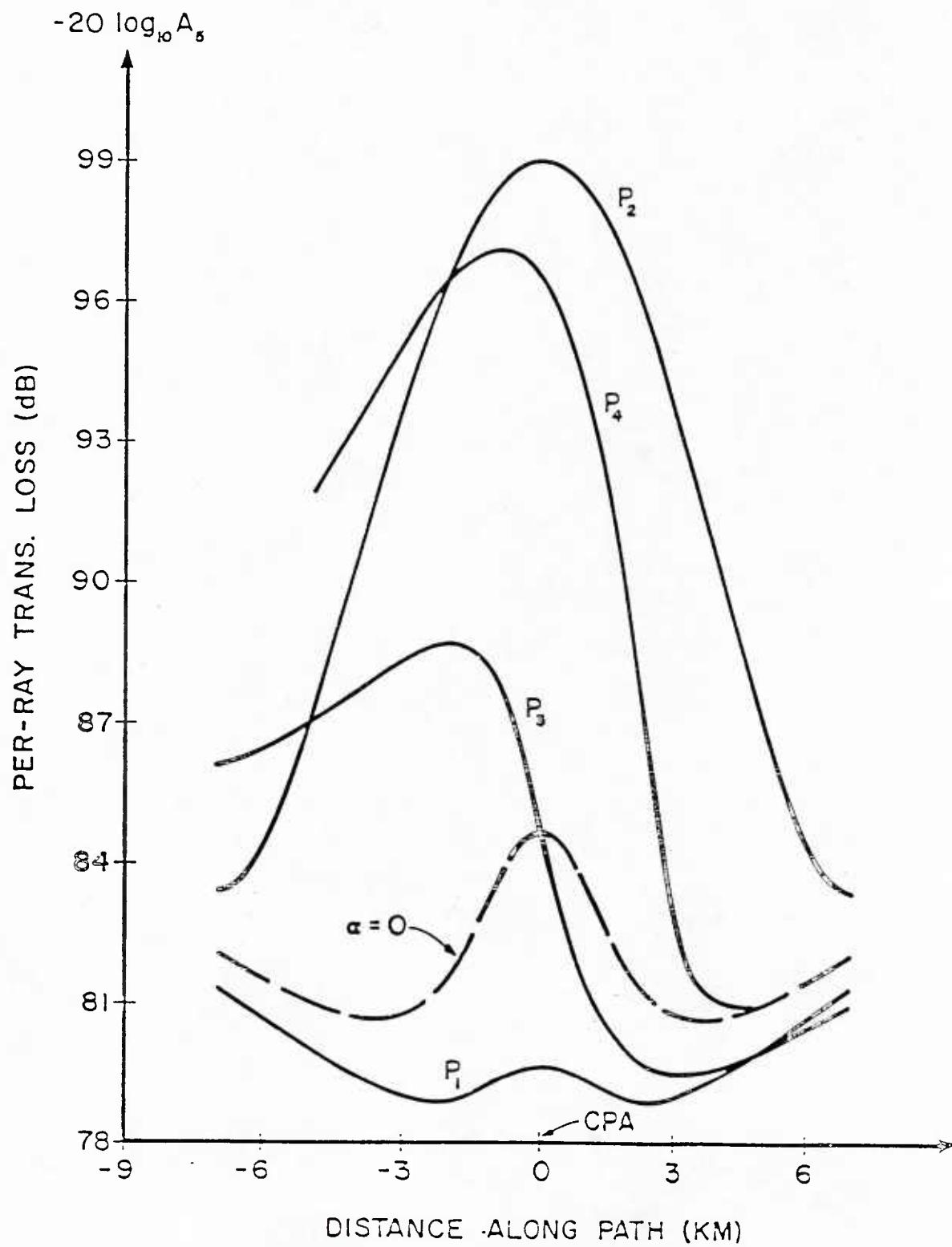
FIGURE 6
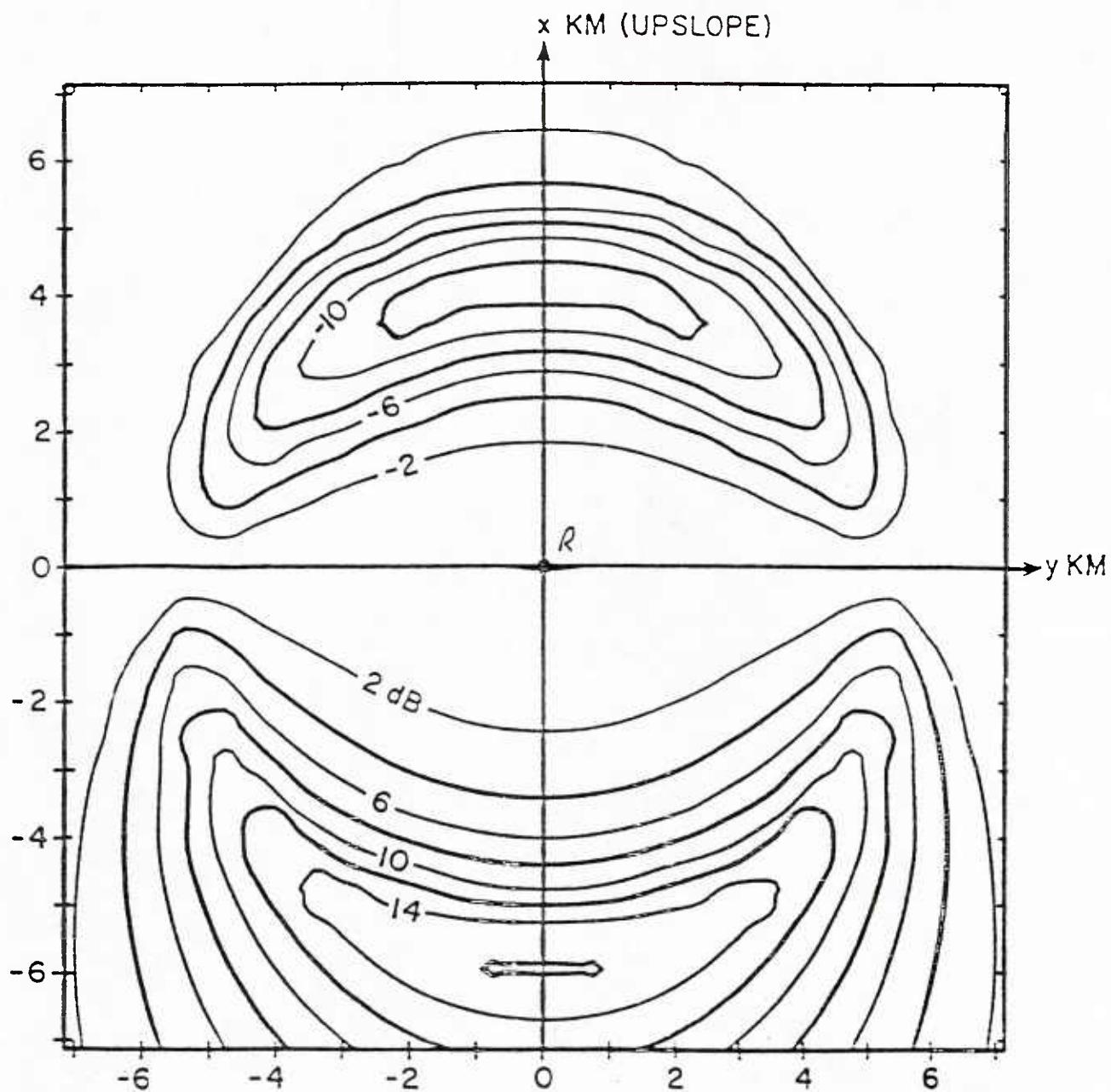
FIGURE 7

FIGURE 8
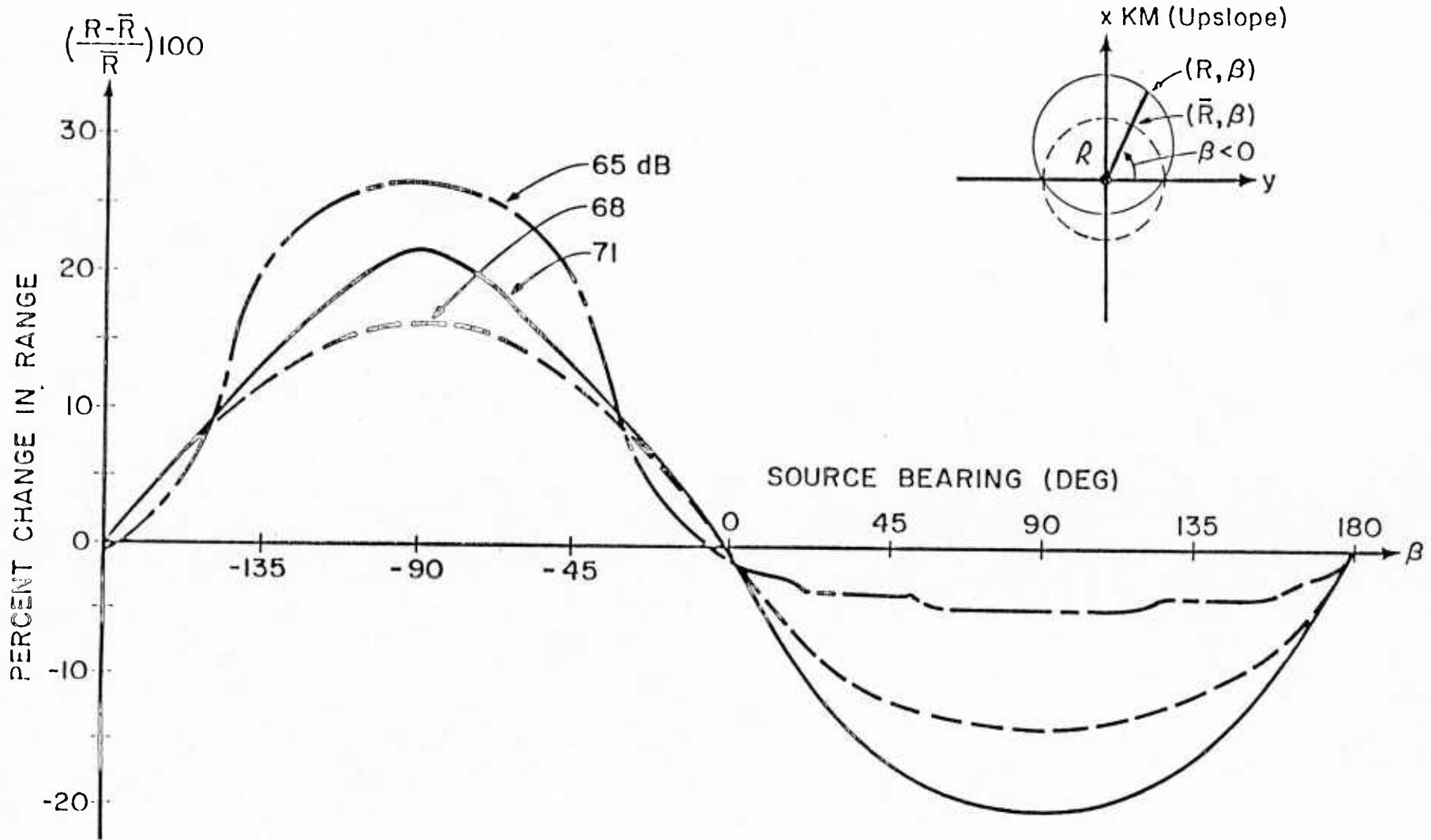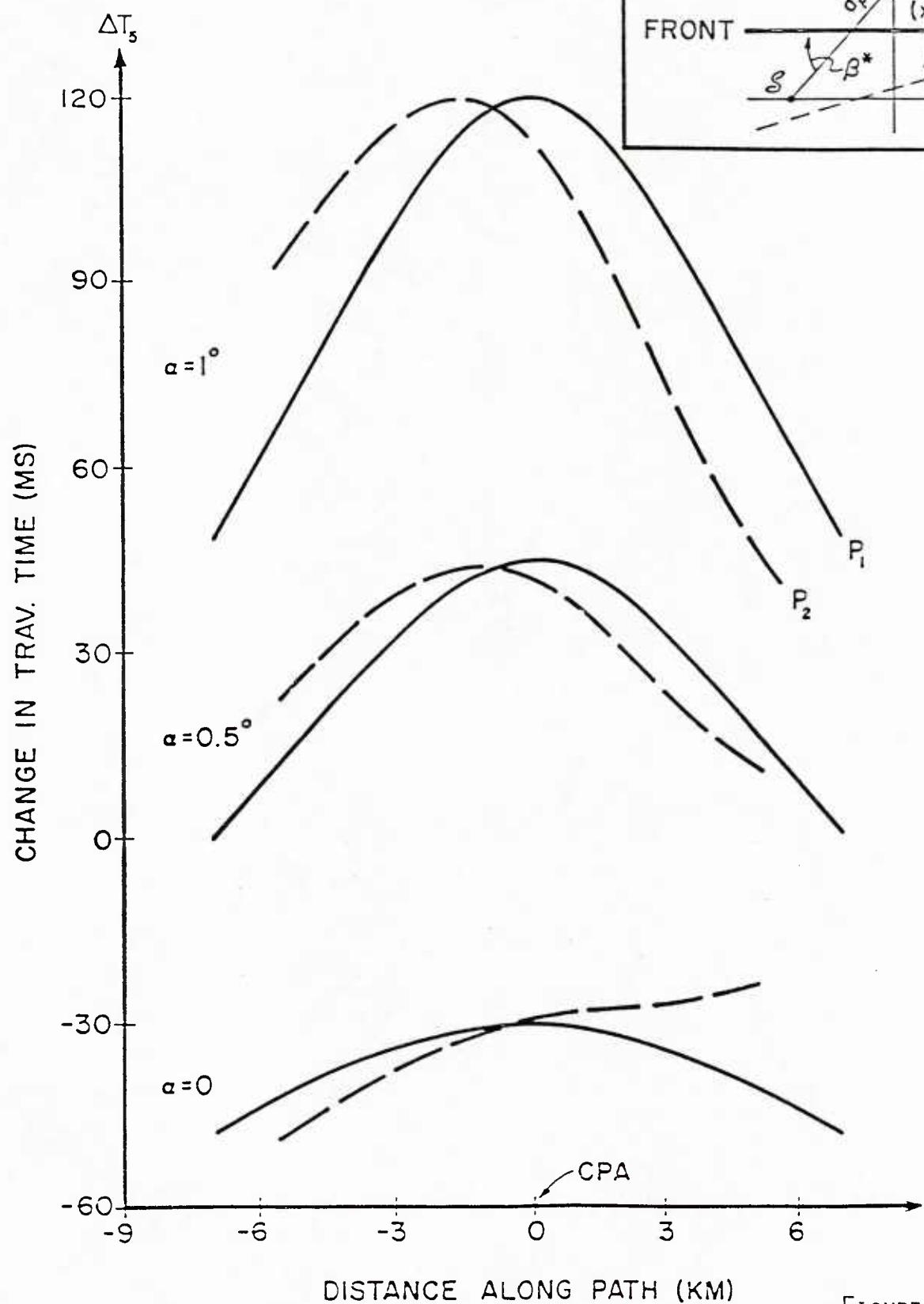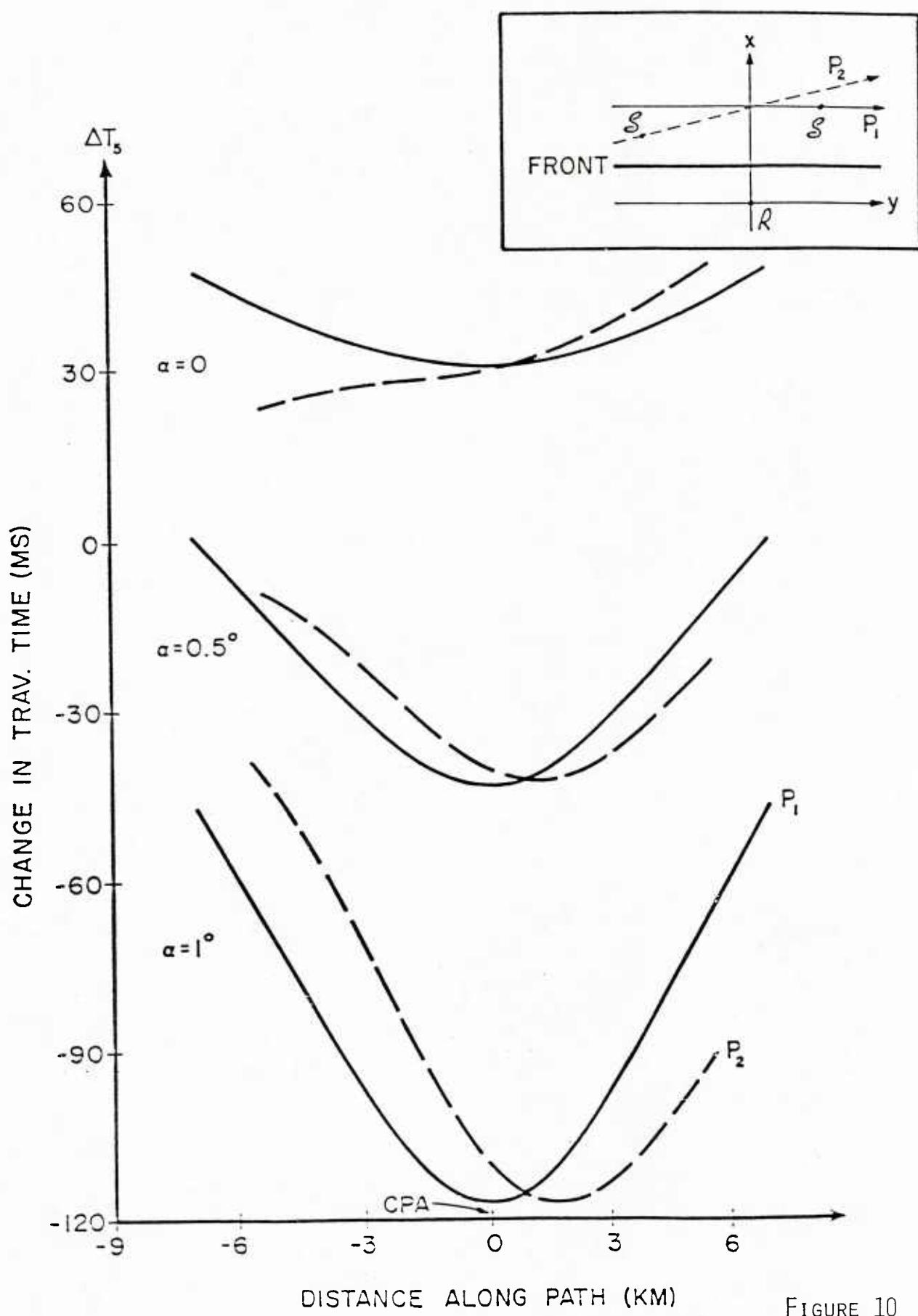
FIGURE 9

FIGURE 10
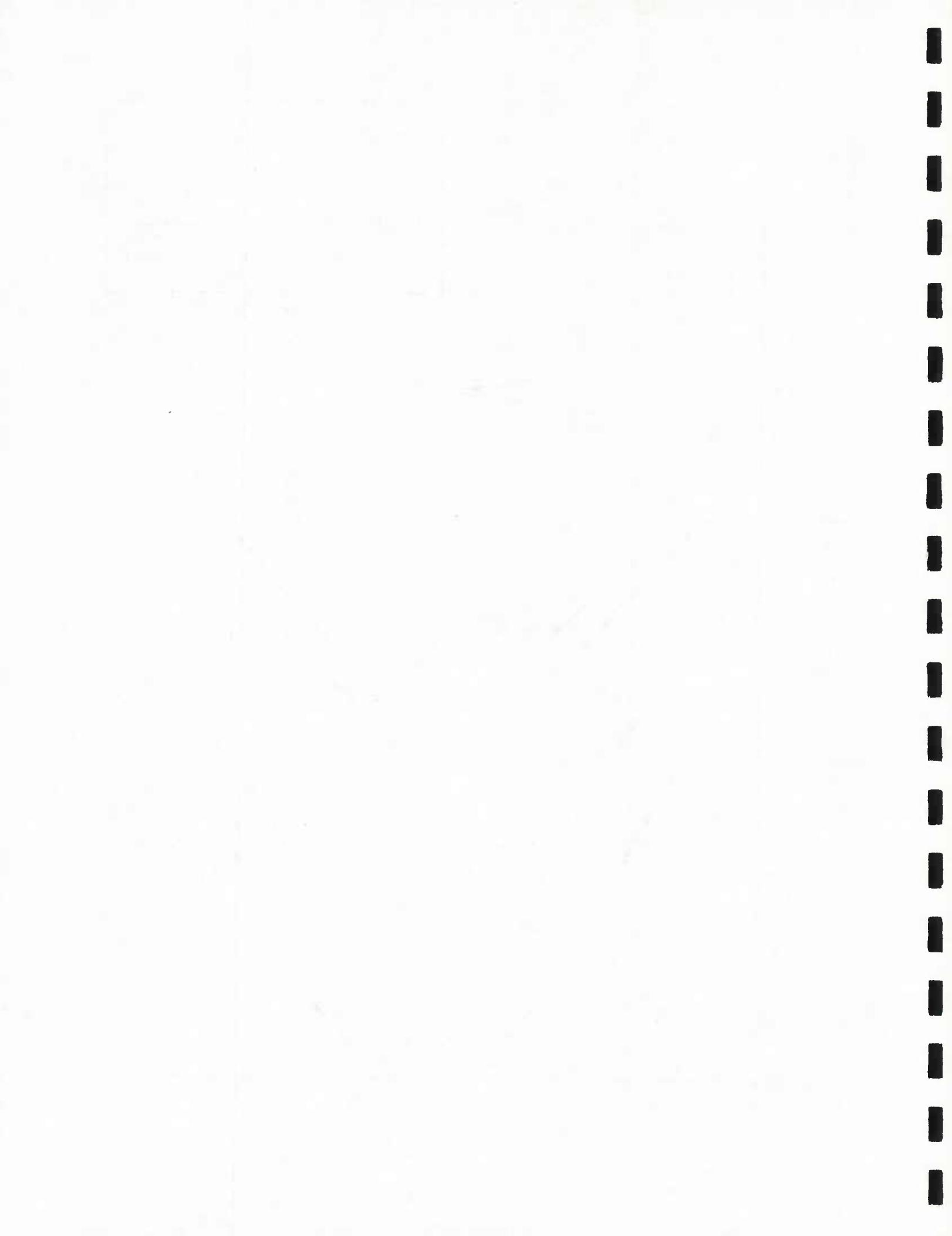
UNCLASSIFIED
DISTRIBUTION LIST
DEC 1981

Addressee	No. of Copies	Addressee	No. of Cop
Office of Naval Research 800 North Quincy Street Arlington, Virginia 22217 Attn: Code 425AC 102 102C 210 220	2 1 1 1 1	Technical Director Naval Oceanographic Research and Development Activity NSTL Station Bay St. Louis, Mississippi 39522 Attn: Technical Director Dr. L. Solomon Dr. R. Gardner Mr. E. Chaika Mr. R. Van Wyckhouse Dr. S. W. Marshall	1 1 1 1 1 1
Office of Naval Technology 800 North Quincy Street Arlington, Virginia 22217 Attn: MAT 0721 MAT 0724	1 1	Director Naval Oceanographic Office NSTL Station Bay St. Louis, Mississippi 39522 Attn: Mr. H. Beck Dr. T. M. Davis Mr. W. H. Geddes Dr. W. Jobst Mr. R. Merrifield Mr. R. A. Peloquin Dr. M. K. Shank	1 1 1 1 1 1 1
Director Naval Research Laboratory 4555 Overlook Avenue, SW. Washington, D.C. 20375 Attn: Dr. J. C. Munson Mr. R. R. Rojas Dr. B. B. Adams Dr. W. B. Moseley Dr. J. P. Dugan Unclassified Library	1 1 1 1 1 1		
Superintendent Naval Research Laboratory Underwater Sound Reference Division P.O. Box 8337 Orlando, Florida 32806	1	Office of the Assistant Secretary of the Navy for Research, Engineering and Systems Washington, D.C. 20350 Attn: Dr. D. Barbe, Rm 4E732 Pentagon Dr. J. H. Probus, Rm 5E779 Pentagon	1 1
Director Office of Naval Research Branch Office 1030 East Green Street Pasadena, California 91106	1	Chief of Naval Operations Room 5D580, Pentagon Washington, D.C. 20350 Attn: OP951F	1
Office of Naval Research Rm 239, Campbell Hall University of California Berkeley, California 94720	1	Commander Naval Sea Systems Command Department of Navy Washington, D.C. 20362 Attn: Capt. James M. Van Metre PMS 409	1
Director Office of Naval Research Branch Office 495 Summer Street Boston, Massachusetts 02210	1	Chief of Naval Operations Office of the Director Naval Oceanographic Division OP-952	
Office of Naval Research New York Area Office 715 Broadway – 5th Floor New York, New York 10003	1	Department of the Navy Washington, D.C. 20352 Attn: Dr. R. W. James Capt. J. C. Harlett	1 1
Commanding Officer Office of Naval Research Branch Office Box 39 FPO New York 09510	1	Commander Oceanographic System, Atlantic Box 100 Norfolk, Virginia 23511	1
Director Office of Naval Research Branch Office 536 South Clark Street Chicago, Illinois 60605	1	Commander Oceanographic System, Pacific Box 1390 Pearl Harbor, Hawaii 96860	1
Office of Naval Research Resident Representative University District Building, Room 422 1107 North East 45th Street Seattle, Washington 98105	1		

Addressee	No. of Copies
Defense Advanced Research Projects Agency 1400 Wilson Boulevard Arlington, Virginia 22209 Attn: Capt. V. Simmons	1
ARPA Research Center Moffett Field Unit #1 California 94035 Attn: Mr. E. Smith	1
Commanding Officer Fleet Weather Central Box 113 Pearl Harbor, Hawaii 96860	1
Naval Ocean Systems Center (Kaneohe) Kaneohe, Hawaii 96863 Attn: Mr. D. Hightower Mr. B. Kishimoto Mr. R. Buecher	1 1 1
Commander Naval Electronic Systems Command 2511 Jefferson Davis Highway National Center #1 Arlington, Virginia 20360 Attn: CAPT C. A. Rose,, PME 124 LCDR P. Girard, NAVELEX 612	2
Commander Naval Air Systems Command Jefferson Plaza #1 1411 Jefferson Davis Highway Arlington, Virginia 20360	1
Commander Naval Sea Systems Command National Center #2 2521 Jefferson Davis Highway Arlington, Virginia 20362 Attn: SEA 63R 63Y	1 1
Commanding Officer Fleet Numerical Weather Central Monterey, California 93940 Attn: Mr. Paul Stevens Dr. D.R. McLain (NMFS)	1 1
Defense Documentation Center Cameron Station Alexandria, Virginia 22314	12
Commander Naval Ocean Systems Center Department of the Navy San Diego, California 92132 Attn: Dr. Daniel Andrews Dr. Dean Hanna Mr. Henry Aurand Dr. Harry A. Schenck	1 1 1 1

Addressee	No. of Cop
Commander Naval Surface Weapons Center Acoustics Division Silver Spring, Maryland 20910	1
Commander Naval Surface Weapons Center Science and Mathematics Research Group (K05) Dahlgren, Virginia 22448 Attn: Dr. E.W. Schwiderski	1
Commanding Officer Naval Underwater Systems Center New London Laboratory New London, Connecticut 06320 Attn: Dr. William Von Winkle Dr. A. Nuttall Mr. A. Ellinthorpe Dr. D.M. Viccione Mr. A. Donn Cobb	1 1 1 1 1
Commander Naval Air Development Center Department of the Navy Warminster, Pennsylvania 18974 Attn: Unclassified Library	1
Commanding Officer Naval Coastal Systems Laboratory Panama City, Florida 32401 Attn: Unclassified Library	1
Commanding Officer Naval Underwater Systems Center Newport Laboratory Newport, Rhode Island 02840 Attn: Unclassified Library	1
Commander David W. Taylor Naval Ship Research and Development Center Bethesda, Maryland 20084 Attn: Dr. M. Sevik	1
Superintendent Naval Postgraduate School Monterey, California 93940	1
Superintendent U.S. Naval Academy Annapolis, Maryland 21402 Attn: Library	1
Commanding Officer Naval Intelligence Support Center 4301 Suitland Road Washington, D.C. 20390 Attn: NISC 20	1
Director Applied Physics Laboratory University of Washington 1013 North East 40th Street Seattle, Washington 98105 Attn: Dr. T.E. Ewart Dr. M. Schulkin	1 1

Addressee	No. of Copies
Applied Research Laboratories University of Texas at Austin P.O. Box 8029 10000 FM Road 1325 Austin, Texas 78712 Attn: Dr. Loyd Hampton Dr. Charles Wood	 1 1
Atlantic Oceanographic and Meteorological Laboratories 15 Rickenbacker Causeway Miami, Florida 33149 Attn: Dr. John Proni	 1
Bell Telephone Laboratories 1 Whippany Road Whippany, New Jersey 07981 Attn: Dr. Bruce Bogart Dr. Peter Hirsch	 1 1
Bolt, Beranek, and Newman, Inc. 50 Moulton Street Cambridge, Massachusetts 02238 Attn: Dr. K. L. Chandiramani	 1
Chase, Inc. 14 Pinckney Street Boston, Massachusetts 02114 Attn: Dr. David Chase	 1
Dr. David Middleton 127 East 91st Street New York, New York 10028	 1
Duke University Department of Electrical Engineering Durham, North Carolina 27706 Attn: Dr. Loren Nolte	 1
General Electric Company Heavy Military Electronic Systems Syracuse, New York 13201 Attn: Mr. Don Winfield	 1
General Electric Company P.O. Box 1088 Schenectady, New York 12301 Attn: Dr. Thomas G. Kincaid	 1
Gould, Incorporated Chesapeake Instrument Division 6711 Baymeadow Drive Glen Burnie, Maryland 21061 Attn: Dr. O. Lindemann	 1
G R Associates, Inc. 10750 Columbia Pike Suite 602 Silver Spring, Maryland 20901 Attn: Dr. Sheldon Gardner Dr. Frank Rees	
Hughes Aircraft Company P.O. Box 3310 Fullerton, California 92634 Attn: Mr. S. W. Autrey	 1

Addressee	No. of Copies
Hydroacoustics, Inc. 321 Northland Ave. P.O. Box 3818 Rochester, New York 14610	 1

Institute for Acoustical Research
Miami Division for the Palisades
  Geophysical Institute
615 South West 2nd Avenue
Miami, Florida 33130
Attn: Mr. M. Kronengold
    Dr. J. Clark
	
	1
	1

Institute of Geophysics and Planetary
  Physics
Scripps Institute of Oceanography
University of California
La Jolla, California 92093
Attn: Dr. W. Munk
    Mr. J. Spiesberger
	
	1
	1

Jaycor Incorporated 205 South Whiting Street Suite 607 Alexandria, Virginia 22304 Attn: Dr. S. Adams	 1
Massachusetts Institute of Technology Acoustics and Vibration Laboratory 70 Massachusetts Avenue Room 5-222 Cambridge, Massachusetts 02139 Attn: Professor Patrick Leehey	 1
Palisades Sofar Station Bermuda Division of Palisades Geophysical Institute FPO New York 09560 Attn: Mr. Carl Hartdegen	 1
Polar Research Laboratory 123 Santa Barbara Avenue Santa Barbara, California 93101 Attn: Mr. Beaumont Buck	 1
Research Triangle Institute Research Triangle Park Durham, North Carolina 27709 Attn: Dr. S. Huffman	 1
Rensselaer Polytechnic Institute Troy, New York 12181 Attn: Dr. Melvin J. Jacobson	
Science Applications, Inc. 8400 Westpark Drive McLean, Virginia 22102 Attn: Dr. P. Tatro	
S.D.P. Inc. 15250 Ventura Boulevard Suite 518 Sherman Oaks, California 91403 Attn: Dr. M. A. Basin	 1